

Research Paper

Astrocytic YAP protects the optic nerve and retina in an experimental autoimmune encephalomyelitis model through TGF- β signaling

Qian Wu^{1,2#}, Xuemeng Miao^{2#}, Jingjing Zhang^{5#}, Ludan Xiang², Xiuchun Li⁴, Xiaomei Bao⁵, Siyu Du², Mianxian Wang⁵, Shuangda Miao⁴, Yiren Fan², Wei Wang², Xingxing Xu⁵, Xiya Shen⁵, Danlu Yang⁵, Xiwu Wang⁵, Yuanyuan Fang², Lixin Hu², Xuyi Pan⁴, Haoru Dong⁴, Hui Wang⁴, Ying Wang^{3✉}, Jia Li^{4✉}, Zhihui Huang^{1,2,4✉}

1. School of pharmacy and Holistic Integrative Pharmacy Institutes, Hangzhou Normal University, Hangzhou, Zhejiang, 311121, China.
2. School of Mental Health, Wenzhou Medical University, Wenzhou, Zhejiang, 325035, China.
3. Phase I Clinical Research Center, Zhejiang Provincial People's Hospital of Hangzhou Medical College, Hangzhou, Zhejiang, 310053, China.
4. The First Affiliated Hospital of Wenzhou Medical University, Wenzhou, Zhejiang, 325035, China.
5. School of Basic Medical Sciences, Wenzhou Medical University, Wenzhou, Zhejiang, 325035, China.

These authors contribute equally: Qian Wu, Xuemeng Miao, Jingjing Zhang

✉ Corresponding authors: Ying Wang, Email: nancywangying@163.com. Jia Li, Email: susannita@126.com. Zhihui Huang, Email: huang0069@hznu.edu.cn.

© The author(s). This is an open access article distributed under the terms of the Creative Commons Attribution License (<https://creativecommons.org/licenses/by/4.0/>). See <http://ivyspring.com/terms> for full terms and conditions.

Received: 2021.03.03; Accepted: 2021.07.06; Published: 2021.07.25

Abstract

Rationale: Optic neuritis is one of main symptoms in multiple sclerosis (MS) that causes visual disability. Astrocytes are pivotal regulators of neuroinflammation in MS, and astrocytic yes-associated protein (YAP) plays a critical role in neuroinflammation. Meanwhile, YAP signaling is involved in visual impairment, including glaucoma, retinal choroidal atrophy and retinal detachment. However, the roles and underlying mechanisms of astrocytic YAP in neuroinflammation and demyelination of MS-related optic neuritis (MS-ON) remains unclear.

Methods: To assess the functions of YAP in MS-ON, experimental autoimmune encephalomyelitis (EAE, a common model of MS) was established, and mice that conditional knockout (CKO) of YAP in astrocytes, YAP^{GFAP}-CKO mice, were successfully generated. Behavior tests, immunostaining, Nissl staining, Hematoxylin-Eosin (HE) staining, TUNEL staining, Luxol Fast Blue (LFB) staining, electron microscopy (EM), quantitative real-time PCR (qPCR), gene set enrichment analysis (GSEA) and gene set variation analysis (GSVA) by RNA sequencing were used to examine the function and mechanism of YAP signaling based on these YAP^{GFAP}-CKO mice and EAE model mice. To further explore the potential treatment of YAP signaling in EAE, EAE mice were treated with various drugs, including SRI-011381 that is an agonist of transforming growth factor- β (TGF- β) pathway, and XMU-MP-1 which inhibits Hippo kinase MST1/2 to activate YAP.

Results: We found that YAP was significantly upregulated and activated in the astrocytes of optic nerve in EAE mice. Conditional knockout of YAP in astrocytes caused more severe inflammatory infiltration and demyelination in optic nerve, and damage of retinal ganglion cells (RGCs) in EAE mice. Moreover, YAP deletion in astrocytes promoted the activation of astrocytes and microglia, but inhibited the proliferation of astrocytes of optic nerve in EAE mice. Mechanically, TGF- β signaling pathway was significantly down-regulated after YAP deletion in astrocytes. Additionally, both qPCR and immunofluorescence assays confirmed the reduction of TGF- β signaling pathway in YAP^{GFAP}-CKO EAE mice. Interestingly, SRI-011381 partially rescued the deficits in optic nerve and retina of YAP^{GFAP}-CKO EAE mice. Finally, activation of YAP signaling by XMU-MP-1 relieved the neuroinflammation and demyelination in optic nerve of EAE mice.

Conclusions: These results suggest astrocytic YAP may prevent the neuroinflammatory infiltration and demyelination through upregulation of TGF- β signaling and provide targets for the development of therapeutic strategies tailored for MS-ON.

Key words: optic neuritis; astrocytes; YAP; TGF- β 1; neuroinflammation

Introduction

Multiple sclerosis (MS) is the most common demyelinating disease of the central nervous system (CNS) [1], and optic neuritis, one of the main symptoms of MS [2], forces 30% of MS patients to seek medical treatments in the initial course and affects 70% of ones in the later course [3]. It manifests as acute reductions of visual field size, color vision, central visual acuity, and afferent pupillary function [4], which impacts the quality of life seriously [5]. But until now, there has been no effective treatment for permanent vision loss or trauma caused in MS-related optic neuritis (MS-ON) [6].

MS-ON, a kind of immune inflammatory disorder, can lead to neuroinflammation and demyelination of optic nerve, axonal damage and loss, and retinal ganglion cells (RGCs) death. Experimental autoimmune encephalomyelitis (EAE) has been used as a common model of MS to study the mechanism of MS-ON [4, 7]. Nowadays, several studies have shown that astrocytes play important roles in immune inflammatory disorders [8]. For example, inhibition of astrocytic NF- κ B has recently been reported to improve functional outcome in EAE mice [9]. The importance of astrocytes in immune inflammatory disorders is further supported by recent clinical evidence that the majority of patients with neuromyelitis optica, a CNS inflammatory disease with similarities to MS, have autoantibodies to aquaporin-4, a molecule expressed in CNS only on astrocyte foot processes [10], and that the severity of clinical signs in such patients correlates with aquaporin-4-specific antibody titers [11]. Furthermore, previous studies have shown that a loss or disruption of barrier functions of scar-forming reactive astrocytes may represent a pathophysiological mechanism that could precipitate or exacerbate CNS pathology in acquired immune inflammatory disorders of the CNS, including MS or related conditions [12, 13]. Functionally, astrocytes are activated and proliferate, which contributes to regulating demyelination of the axons and plays a significant role in neuroinflammation of EAE [14]. However, the detailed roles and underlying mechanisms of astrocytes in the neuroinflammation and demyelination of MS-ON remains unclear.

Yes-associated protein (YAP) and its paralog, transcriptional coactivators with PDZ-binding motif (TAZ), which is also known as WW Domain Containing Transcription Regulator 1 (WWTR1), control cell proliferation, tissue homeostasis, and organ size [15, 16], and act as transcriptional co-activators that are known to be downstream effectors of the conserved Hippo kinase pathway [17,

18]. Previous studies have reported that YAP plays critical roles in regulating proliferation and differentiation of astrocytes [19-21] and has a tremendous impact on Schwann cell myelination [22] and neuroinflammation [23]. Additionally, YAP signaling is involved in vision-related diseases such as glaucoma, retinal choroidal atrophy and retinal detachment [24-26]. However, it remains unknown whether YAP participates in MS-ON and its functions on the activated astrocytes, demyelination and neuroinflammation.

Additionally, transforming growth factor- β (TGF- β) is a multifunctional regulator of cell activity, which plays an important role in regulating the function of inflammatory immune cells and myelination [27-29]. Some studies have shown that the expression of TGF- β was significantly elevated in EAE mice [30]. In EAE mice model, overexpression of TGF- β could attenuate the incidence and severity of EAE notably [31-33]. However, the role of TGF- β is cell type-dependent, and the combined effect of different factors makes the biological effects of TGF- β more complicated [34, 35]. Recent studies have shown that YAP expression was elevated in HSCT6 cells treated with TGF- β , and promoted the activation and proliferation of HSCT6 cells [36]. TGF- β can restrain nuclear translocation of YAP/TAZ at the mRNA and protein levels [37], while YAP can regulate the cell response of TGF- β effectively [38]. However, the interaction between YAP and TGF- β in MS-ON remains unclear.

Results of the present study demonstrated that YAP in astrocytes was activated and upregulated in optic nerve of EAE mice, and conditional ablation of YAP in astrocytes aggravated inflammatory infiltration and demyelination, and resulted into more astrocytic and microglial activation in optic nerve and retina of EAE mice, associated with a drastic increasing of RGCs loss in retina of EAE mice. Mechanistically, YAP signaling prevented demyelination and inflammatory response through TGF- β pathways. Our study reveals the underlying mechanisms of demyelination and inflammation controlled by astrocytes in optic neuritis, which may help to develop new strategies for the treatment of MS-ON.

Material and Methods

Mouse breeding and genotyping

YAP^{GFAP}-CKO mice were generated by crossing floxed YAP allele (YAP^{f/f}) with GFAP-Cre transgenic mice. The origin of our GFAP-Cre mice is GFAP-Cre 8Gtm (from Jackson Labs), and YAP^{f/f} mice were generated as previously described [39]. YAP^{f/f} and

YAP^{GFAP}-CKO mice were maintained in the background of C57BL/6 strain and identified by genotyping. All mice were divided into experimental groups randomly. Additionally, genotyping and experimental condition sets were performed blindly. Moreover, the histological and behavioral tests were conducted with strict compliance to the relevant regulations of Animal Bioethics Committee of Hangzhou Normal University and Wenzhou Medical University.

Establishment of EAE model

EAE model was performed as described previously [40]. Briefly, female C57BL/6 mice (8-10 weeks) were anesthetized and then subcutaneously immunized with 0.2 mg of myelin oligodendrocyte glycoprotein 35-55 (MOG₃₅₋₅₅) [GL Biochem (Shanghai) Ltd] emulsified (1:1) in Freund's complete adjuvant containing 8 mg/ml mycobacterium tuberculosis (strain H37RA, Difco, Detroit, Michigan, USA). Mice were divided into 2 groups: the mice in control group received subcutaneous injection of phosphate-buffered saline (PBS), while the mice in the model experiment (EAE) group were injected subcutaneously with the MOG₃₅₋₅₅/Freund's complete adjuvant emulsion in PBS. Furthermore, the mice were intraperitoneally injected with 300 ng of pertussis toxin (Sigma, USA) on day 0 and 2 after immunization. All injection and scoring processes were double-blinded. From 0 to 22 days post injection (dpi), body weight was recorded and the neurological function was assessed according to five-point scoring criteria published previously (All animals were examined and scored daily for clinical signs of EAE). Animals were clinically graded as follows: 0 = no signs, 1 = loss of tail tonicity, 2 = loss of tail tonicity and mild paralysis of hindlimbs, 3 = paralysis of hindlimbs, 4 = hindlimb paralysis and mild paralysis of forelimbs and 5 = complete paralysis or death. All mice were sacrificed at 22 dpi [41].

Injection of drugs and reagents

After EAE induction, SRI-011381 (HY-100347A, MCE), dissolved in saline containing DMSO (10%) and PEG300 (40%), was injected intraperitoneally into mice at a dose of 30 mg/kg every 2 d [42]. XMU-MP-1 (HY-100526, MCE) was dissolved in DMSO and injected intraperitoneally at a dose of 1 mg/kg, given every 2 d [43]. At the end of the study, the optic nerve and retina were collected for further investigations.

Hematoxylin-Eosin (HE) staining

Briefly, after perfusion with PBS and then with 4% paraformaldehyde (PFA), the optic nerve and retina tissues were immersed in 4% PFA for 24 h and transferred to 30% sucrose solution until they sank.

Subsequently, the optic nerve and retina tissues were embedded in optimal cutting temperature and a cryostat (Thermo, USA) was used to cut into a 5 µm-thick longitudinal section of optic nerve and a 10 µm-thick cross section of retina. After dyeing with hematoxylin for 1.5 min, the sections were rinsed with double distilled water for 3 times. Then the sections were incubated in acidic liquid alcohol for 30 s, stained with eosin for 50 s, then rinsed with 95% ethanol and dehydrated with 100% ethanol, finally removed with xylene and fixed with neutral resin. Additionally, the sections were observed under Olympus SLIDEVIEW™ VS200 microscope (Olympus, Germany). The quantitative analysis of the images was made by Image J.

Nissl staining

Nissl staining was conducted as described previously [43]. Briefly, 10 µm-thick retina tissues were incubated with 0.1% cresyl violet for 6 min at room temperature, slices were rinsed with double distilled water, then dehydrated in 95% and 100% ethanol in succession, clarified with xylene, and ultimately fixed with neutral resin. The sections were observed under Olympus SLIDEVIEW™ VS200 microscope (Olympus, Germany). The quantitative analysis of the image was made by Image J.

TUNEL staining

TUNEL staining of 10 µm-thick retina tissues was conducted to evaluate apoptosis as described previously [44]. After washing with PBS, the tissues were blocked in 5% BSA plus 0.3% Triton X-100 for 1 h at room temperature, and treated with *in situ* detection kit according to the manufacturer's protocol (MK500, TaKaRa Bio Inc, Shiga, Japan) at room temperature for 1.5 h. The sections were then observed under Olympus SLIDEVIEW™ VS200 microscope (Olympus, Germany) and processed by Image J or Adobe Photoshop CC 14.0 software.

Luxol Fast Blue (LFB) staining

LFB staining was conducted as described previously [45]. Briefly, 5 µm-thick optic nerve tissues were stained in LFB staining solution overnight at room temperature. Following the staining, the slices were rinsed in 95% ethanol, washed with distilled water, rinsed in 70% ethanol, and later with distilled water. Next, the slices were counterstained in cresyl violet working solution for 15 s, and then dehydrated in 95% and 100% ethanol in succession, differentiated in xylene until there was no background color. Finally, slices were sealed with neutral resin. The sections were then observed under Olympus SLIDEVIEW™ VS200 microscope (Olympus, Germany). The quantitative analysis of the images

was performed by image J.

Electron Microscopy (EM)

For EM, optic nerve tissues were fixed overnight by immersion in 2.5% glutaraldehyde. Then samples were postfixed with 1% osmium and 1% uranyl acetate for 1 h respectively, dehydrated in ethanol, and embedded in resin. The samples were cut into ultrathin sections to receive staining with uranyl acetate. Finally, the sections were used for capturing images with a Hitachi H-600 EM (HITACHI, Tokyo, Japan).

Cell culture

Primary astrocyte cultures were prepared from the cerebral cortex of P1-P3 YAP^{f/f} and YAP^{GFAP}-CKO mice as described previously [39]. In brief, cerebral neocortex was dissected, chopped and then incubated with 0.125% trypsin (Gibco) at 37 °C for 15 min, and separated into single cell suspension by mechanical destruction. The cells were seeded on culture flasks coated with poly-L-lysine (0.1 mg/ml, Sigma) and cultured with DMEM containing 10% fetal bovine serum (FBS, Gibco). After 6-10 d, the microglia and oligodendrocytes were removed by shaking at 250 rpm for about 5 h. Then astrocytes were isolated and plated into a poly-D-lysine coated Petri dish or cover glass. The purity of GFAP⁺ cells was at least 94%.

Immunostaining

Immunostaining of cultured astrocytes or 5 μm-thick optic nerve tissues or 10 μm-thick retina tissues were conducted as previously described [46]. For cultured cells, briefly, cells were received 3 times of rinses with PBS, and then fixed in 4% PFA for 15 min. Next, after being blocked and permeabilized with 0.1% Triton X-100 in PBS containing 5% bovine serum albumin (BSA) at room temperature for 45 min, cells were incubated with primary antibodies at 4 °C for overnight, rinsing in PBS for 3 times and another incubation with secondary antibodies (Invitrogen, 1:1, 000) at room temperature for 1 h. Primary antibodies included rabbit anti-YAP (ab205270, Abcam, 1:200) and mouse anti-GFAP (MAB360, Millipore, 1:500). After rinsing in PBS for another 3 times, cells were mounted.

The tissues were fixed with fresh 4% PFA after cardiac perfusion for 1 d. All tissues were dehydrated in PBS with 30% sucrose until they sank, and sliced on frozen microtome. After washing for 3 times, 5 μm-thick longitudinal sections of optic nerve and 10 μm-thick cross sections of retina were then blocked at room temperature for 1 h in 5% BSA plus 0.3% Triton X-100, incubated with the primary antibody overnight at 4 °C, rinsed with PBS for 3 times and incubated with the corresponding secondary antibodies

(Invitrogen, 1:1, 000) at room temperature for 1 h. The primary antibodies included mouse anti-YAP (WH0010413M1, Sigma, 1:200), rabbit anti-YAP (ab205270, Abcam, 1:500), rabbit anti-GFAP (ab68428, Abcam, 1:250), mouse anti-GFAP (MAB360, Millipore, 1:500), goat anti-Iba1 (ab5076, Abcam, 1:500), rabbit anti-Ki67 (AB9260, Millipore, 1:300), mouse anti-PH3 (ab14955, Abcam, 1:500), rabbit anti-CD45 (ab10558, Abcam, 1:500), rabbit anti-CD206 (ab125028, Abcam, 1:200), mouse anti-MBP (ab62631, Abcam, 1:500), rabbit anti-RBPMS (GTX118619, GeneTex, 1:500), rabbit anti-NeuN (ab177487, Abcam, 1:200), mouse anti-NeuN (ab104224, Abcam, 1:200), rabbit anti-TGF-β1 (ab215715, Abcam, 1:200) and rabbit anti-Vimentin (ab92547, Abcam, 1:800). Sections were stained for DAPI (Sigma, 1:1, 000) to visualize nucleus. Images were visualized by Olympus SLIDEVIEW™ VS200 microscope (Olympus, Germany) and processed by Image J or Adobe Photoshop CC 14.0 software. No positive signal was observed in the control group.

Immunohistochemistry

The antigens were prepared using Sodium Citrate Antigen Retrieval Solution for 30 min at 90 °C. Subsequently, the endogenous peroxidase activity of sections was blocked with 3% H₂O₂ for 0.5 h and 5% BSA plus 0.3% Triton X-100 at room temperature for 1 h. Following blocking, the sections were incubated with rabbit anti-YAP antibody (ab205270, Abcam, 1:200) overnight at 4 °C, and then washed 3 times with PBS and incubated for 1 h with HRP-conjugated goat anti-rabbit IgG (Abcam, 1:100). Immunoreactivity was detected by using diaminobenzidine. All antibodies used for immunohistochemistry were diluted in PBS containing 5% BSA. The sections were then observed under Olympus SLIDEVIEW™ VS200 microscope (Olympus, Germany). The brown yellow particles in the nucleus were judged as YAP positive (YAP⁺) cells. No positive signal was observed in the control group.

RNA sequencing and functional enrichment analysis

Total RNA was extracted from cultured YAP^{+/+} and YAP^{-/-} astrocytes as well as optic nerve of control and EAE mice using Trizol reagent (Invitrogen), according to the manufacturer's protocol. The RNA samples used for sequencing were with A260:A280 ratio above 1.8, A260:A230 ratio above 2.0 and the RNA integrity number above 7.0. Briefly, rRNAs were removed from total RNA using Ribo-Zero rRNA Removal Kit (Epicentre, USA) and fragmented to approximately 200 bp. Subsequently, the purified RNAs were subjected to first strand and second strand cDNA synthesis following by adaptor ligation

and enrichment with a low-cycle according to instructions of NEBNext® Ultra™ RNA Library Prep Kit for Illumina (NEB, USA). The purified library products were evaluated using the Agilent 2200 Tape Station and Qubit®2.0 (Life Technologies, USA) and then diluted to 10 pM for cluster generation *in situ* on the pair-end flow cell followed by HiSeq3000sequencing (2×150 bp). The clean reads were obtained after removal of reads containing adapter, ploy-N and at low quality from raw data. HISAT2 was used to align the clean reads to the mouse reference genome mm10 with default parameters. HTSeq was subsequently employed to convert aligned short reads into read counts for each gene model. Differential expression was assessed by DESeq using read counts as input. The Benjamini-Hochberg multiple test correction method was enabled. Gene set enrichment analysis (GSEA) was performed with all expressed genes using GSEA software (version 4.0.2). Gene sets with normal p-value < 0.05 and FDR < 0.25 were considered significantly enriched. These gene sets were visualized by “ggplot2” (R package). In addition, and “gene set variation analysis (GSVA)” (R package) was utilized to perform GSVA to validate the gene sets of GSEA. The gene set “hall.v7.0.symbols.gmt” was selected as the reference gene set. P-value < 0.05 was considered as statistically significant. Ultimately, “p-heatmap” (R package) was utilized to show the enrichment of all gene sets in each group and the gene expression in the selected gene set.

RNA extraction and quantitative real-time PCR (qPCR)

Total RNA from cells was extracted by using TRIzol™ reagent (#15596026, Ambion) to determine the mRNA expression levels of genes according to protocol provided by the manufacturer. The total RNA (2 µg) was reversely transcribed into cDNA with a SuperScript™ One-Step Reverse Transcription Kit (#10928-034, Invitrogen). The expression levels of TGF-β1, Smad1, Smad2, Smad3, Smad4, Ccl8, Ccl9, IL-1β and TNF-α mRNA were quantified by iTaq™ Universal SYBR® Green Supermax (#172-5122, Bio-Rad) on Real-Time PCR detection System (Applied Biosystems, USA), which using β-actin as the endogenous control. The relative levels of mRNA expression were represented as $\Delta Ct = Ct \text{ gene} - Ct \text{ reference}$, and the multiple change of gene expression was calculated by the $2^{-\Delta\Delta Ct}$ method. The primers used in this research were synthesized by Sang on Biotech, presented below:

TGF-β1 primer: forward, 5'-TGGAGCAACATGTGGAAGCTC-3' and reverse, 5'-GTCAGCAGCCGGTTACCA-3'; Smad1 primer: forward, 5'-GCCGGT

GCAGCTTGAAAATC-3' and reverse, 5'-GCACTGCTCACCTTCACGA-3'; Smad2 primer: forward, 5'-AAGCCATCACCCTCAGAATG-3' and reverse, 5'-CACTGATCTACCGTATTTGCTGT-3'; Smad3 primer: forward, 5'-CACGCAGAACGTGAACAAC-3', and reverse, 5'-GGCAGTAGATAACGTGAGGGA-3'; Smad4 primer: forward, 5'-ACACCAACAAGTAACGATGCC-3', and reverse, 5'-GCAAAGGTTTCACTTTCCCA-3'; Ccl8 primer: forward, 5'-TTC TTTCCTGCTGCTCATA-3', and reverse, 5'-GCAGGTGACTGGAGCCTTAT-3'; Ccl9 primer: forward, 5'-TGGGCCAGATCACACAT-3', and reverse, 5'-TGTGAAACATTTCAATTTCAAGC-3'; IL-1β primer: forward, 5'-GTGTGGATCCAAAGCAATAC-3', and reverse, 5'-GTCTGCTCATTCATGACAAG-3'; TNF-α primer: forward, 5'-GGGGCCACCACGCTCTTCTGTC-3', and reverse, 5'-TGGGCTACGGGCTTGTCCTCG-3'; β-actin primer: forward, 5'-AAGTCCCTCACCTCCCAAAG-3' and reverse 5'-AAGCAATGCTGTCACCTTCCC-3'.

Statistical Analysis

All results were expressed as mean ± SEM derived from at least 3 independent experiments. GraphPad Prism software was used for statistical analysis. Student's t-test, or ANOVA analysis were utilized. $P < 0.05$ was considered as statistically significant.

Results

YAP is upregulated and activated in optic nerve astrocytes of EAE mice

In order to explore potential functions of YAP in MS-ON, EAE, a common typical model of MS, was established. C57BL/6 female mice (8-10 weeks) were immunized with MOG₃₅₋₅₅ and a pertussis toxin boost. As expected, these mice were developed an acute monophasic EAE, and at 22 dpi, the optic nerve and retina of EAE mice were collected. Then LFB staining and myelin basic protein (MBP) (a marker of myelin) immunostaining showed obvious demyelination in optic nerve of EAE mice (Supplementary Figure S1A-D). Furthermore, immunostaining of CD45 (a marker of T cells) and GFAP (a marker of astrocytes) also showed the obvious inflammatory infiltration in optic nerve of EAE mice (Supplementary Figure S1E-H). These results indeed indicated that optic neuritis of EAE model was established successfully.

Next, we examined the expression level of YAP in optic nerve of EAE mice. As shown in Figure 1A-B, compared with control mice, the expression level of YAP was significantly increased in optic nerve of EAE mice. To further examine the cellular expression pattern of YAP in optic nerve, double-immuno-

staining of YAP and several cell markers including GFAP or Iba1 (a marker of microglia) was performed in optic nerve of control mice and EAE mice, respectively, and showed that YAP was mainly expressed in GFAP⁺ astrocytes (Figure 1C), but not in Iba1⁺ microglia (Figure 1E), and YAP was upregulated and displayed the nuclear location in GFAP⁺ astrocytes of EAE optic nerve (Figure 1C-D). Taken together, these results suggest that YAP is upregulated and activated in optic nerve astrocytes of EAE mice.

The normal development of optic nerve and retina in YAP^{GFAP}-CKO mice

To further investigate the role of astrocytic YAP in MS-ON, conditional YAP knockout mice in astrocytes were generated through crossing YAP^{f/f} with GFAP-Cre transgenic mice, namely YAP^{GFAP}-CKO mice (Supplementary Figure S2A-B). Indeed, YAP was knockout in GFAP⁺ astrocytes *in vitro* and *in vivo* (Supplementary Figure S2C-D). However, there was no significant difference in body weight between YAP^{f/f} and YAP^{GFAP}-CKO mice (Supplementary Figure S2E). To further examine whether YAP deletion in astrocytes affected the development of visual system, HE staining was performed and showed that conditional knockout YAP in astrocytes did not significantly affect the

morphology of optic nerve and retina (Supplementary Figure S3A-B). Moreover, immunostaining of GFAP and Iba1 showed that the distribution and number of astrocytes and microglia were not affected in optic nerve by YAP knockout (Supplementary Figure S3C-D). Consistent with the results shown in optic nerve, immunostaining of GFAP, Iba1 and RBPMS (a marker of RGCs) in retina also showed that there were no significant differences in the distribution and number of astrocytes, microglia and RGCs between YAP^{f/f} and YAP^{GFAP}-CKO mice (Supplementary Figure S3E-G). Taken together, these results suggest that YAP deletion in astrocytes does not affect the normal development of optic nerve and retina.

Conditional knockout of YAP in astrocytes exacerbates the demyelination in optic nerve of EAE mice

YAP^{f/f} and YAP^{GFAP}-CKO mice were next injected with MOG₃₅₋₅₅ and pertussis toxin to induce EAE, as shown in Figure 2A, there was no significant difference in body weight between YAP^{f/f} EAE and YAP^{GFAP}-CKO EAE mice. However, deletion of YAP in astrocytes resulted in worse clinical scores. The first clinical signs (tip of tail was limp) were advanced in YAP^{GFAP}-CKO EAE mice, observed at 13-15 and 10-12 dpi, in YAP^{f/f} EAE mice and YAP^{GFAP}-CKO EAE mice, respectively (Figure 2B). Additionally, since

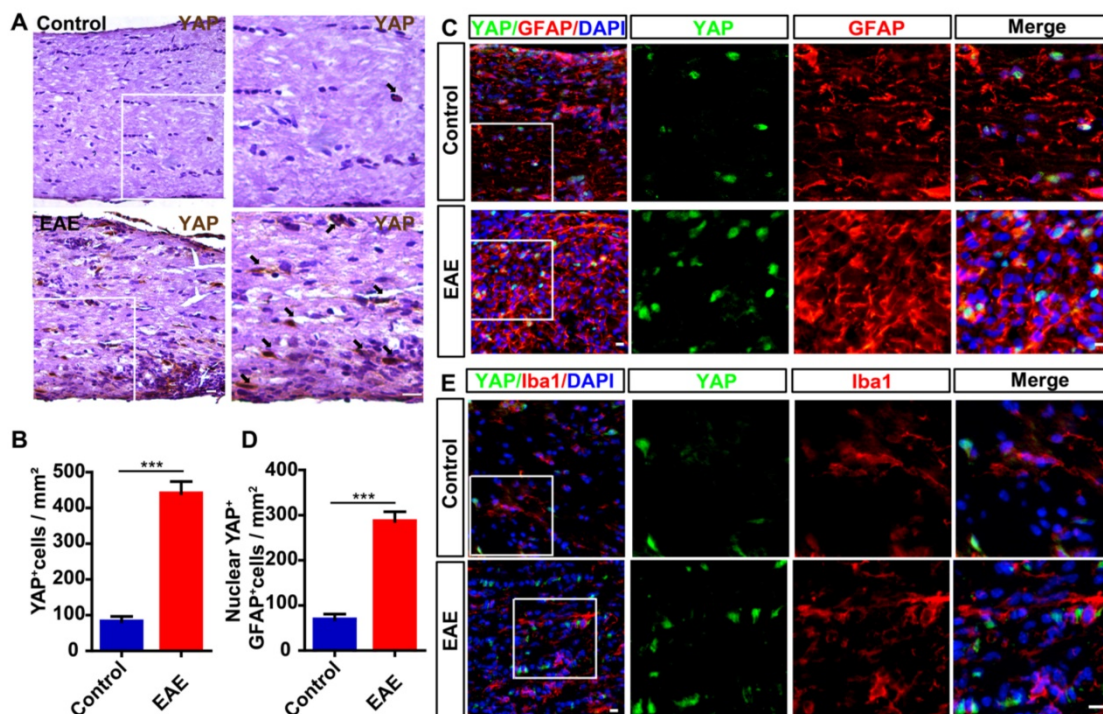


Figure 1. YAP is upregulated and activated in optic nerve astrocytes of EAE mice. (A) Immunohistochemistry detected YAP expression in the optic nerve of control and EAE mice. (B) Quantitative analysis of the density of YAP⁺ cells as shown in (A) (n = 8 per group). (C) Double immunostaining of YAP (green) and GFAP (red) in the optic nerve of control and EAE mice. (D) Quantitative analysis of the density of nuclear YAP⁺ astrocytes as shown in (C) (n = 6 per group). (E) Double immunostaining of YAP (green) and Iba1 (red) in the optic nerve of control and EAE mice. Images of selected regions (white squares) were shown at higher magnification. Data were mean ± SEM, Student's t-test, compared with control group, ***P < 0.001. Scale bars, 20 μm.

demyelination is one of the features of EAE [47], we next examined whether conditional knockout of YAP in astrocytes would affect the demyelination in optic nerve of EAE mice. As expected, LFB staining and MBP immunostaining in optic nerve indeed showed that there was a significant increase in demyelination score and decrease in MBP intensity of YAP^{GFAP}-CKO

EAE mice (Figure 2C-F). Furthermore, EM experiment further showed that YAP^{GFAP}-CKO EAE mice had more severe demyelination phenotype in optic nerve than that in YAP^{fl/fl} EAE mice (Figure 2G-H). Taken together, our results indicate that conditional knockout of YAP in astrocytes exacerbates the demyelination in optic nerve of EAE mice.

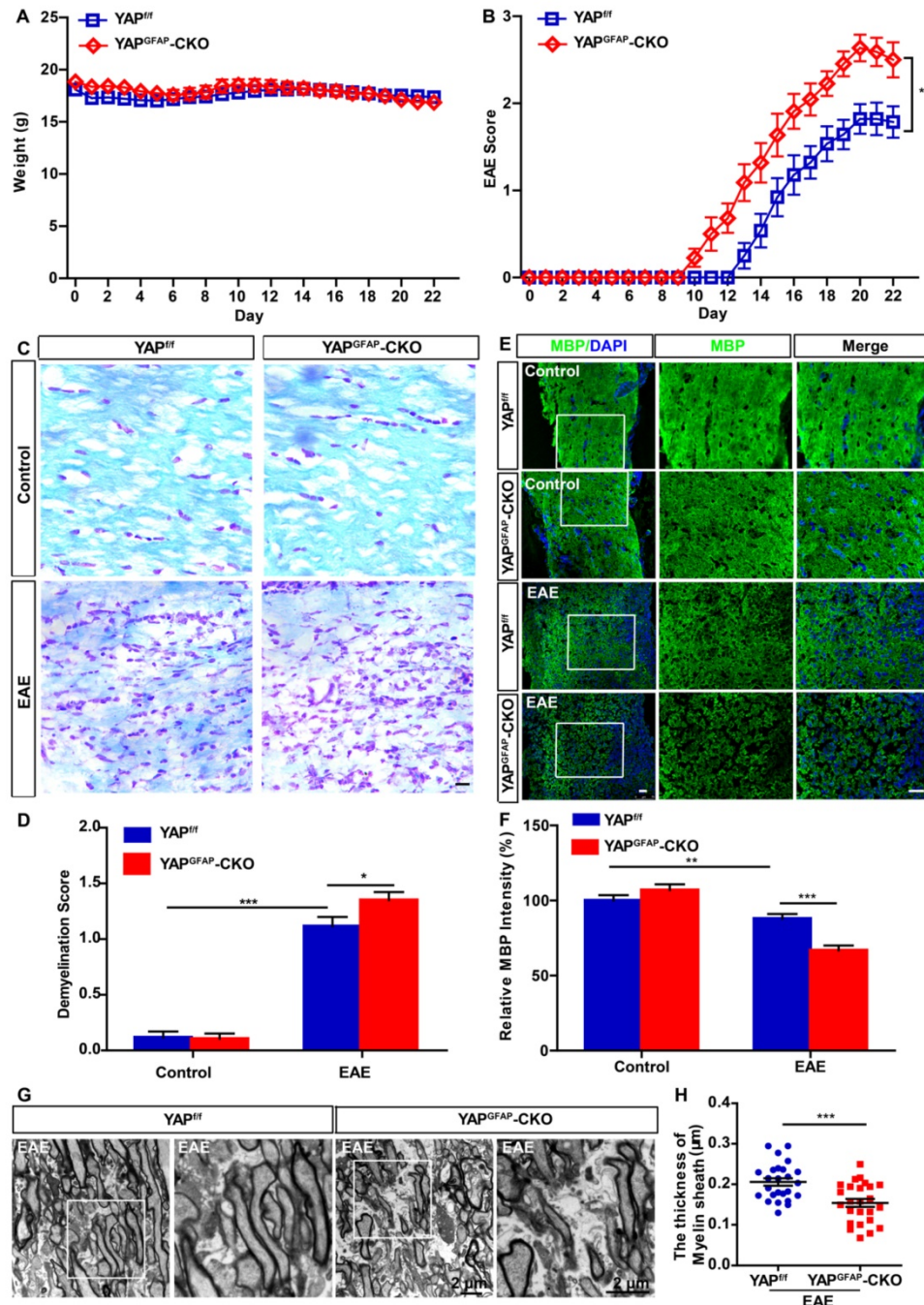


Figure 2. Ablation of YAP in astrocytes exacerbates the demyelination in optic nerve of EAE mice. (A) The body weight of YAP^{fl/fl} (n = 14) and YAP^{GFAP}-CKO (n = 11) mice from 0 to 22 dpi during the process of EAE modeling (two-way ANOVA with Bonferroni's post-tests). (B) The EAE score of YAP^{fl/fl} (n = 14) and YAP^{GFAP}-CKO (n = 11) mice 0 to 22 dpi during the process of EAE modeling (two-way ANOVA with Bonferroni's post-tests). (C) LFB staining of optic nerve obtained from YAP^{fl/fl} and YAP^{GFAP}-CKO mice, YAP^{fl/fl} EAE and YAP^{GFAP}-CKO EAE mice. (D) Quantitative analysis of the demyelination score as shown in (C) (n = 12 per group, two-way ANOVA with Bonferroni's post-tests). (E) Immunostaining of MBP (green) in the optic nerve obtained from YAP^{fl/fl} and YAP^{GFAP}-CKO mice, YAP^{fl/fl} EAE and YAP^{GFAP}-CKO EAE mice. (F) Quantitative analysis of MBP intensity as shown in (E) (n = 12 per group, two-way ANOVA with Bonferroni's post-tests). (G) Transmission EM images of the longitudinal section of the optic nerve obtained from YAP^{fl/fl} EAE and YAP^{GFAP}-CKO EAE mice. (H) Quantitative analysis of the thickness of myelin sheath as shown in (G) (n = 25 per group, Student's t-test). Images of selected regions (white squares) were shown at higher magnification. Data were mean \pm SEM, compared with YAP^{fl/fl} group. * $P < 0.05$, ** $P < 0.01$, *** $P < 0.001$. Scale bars, 20 μ m.

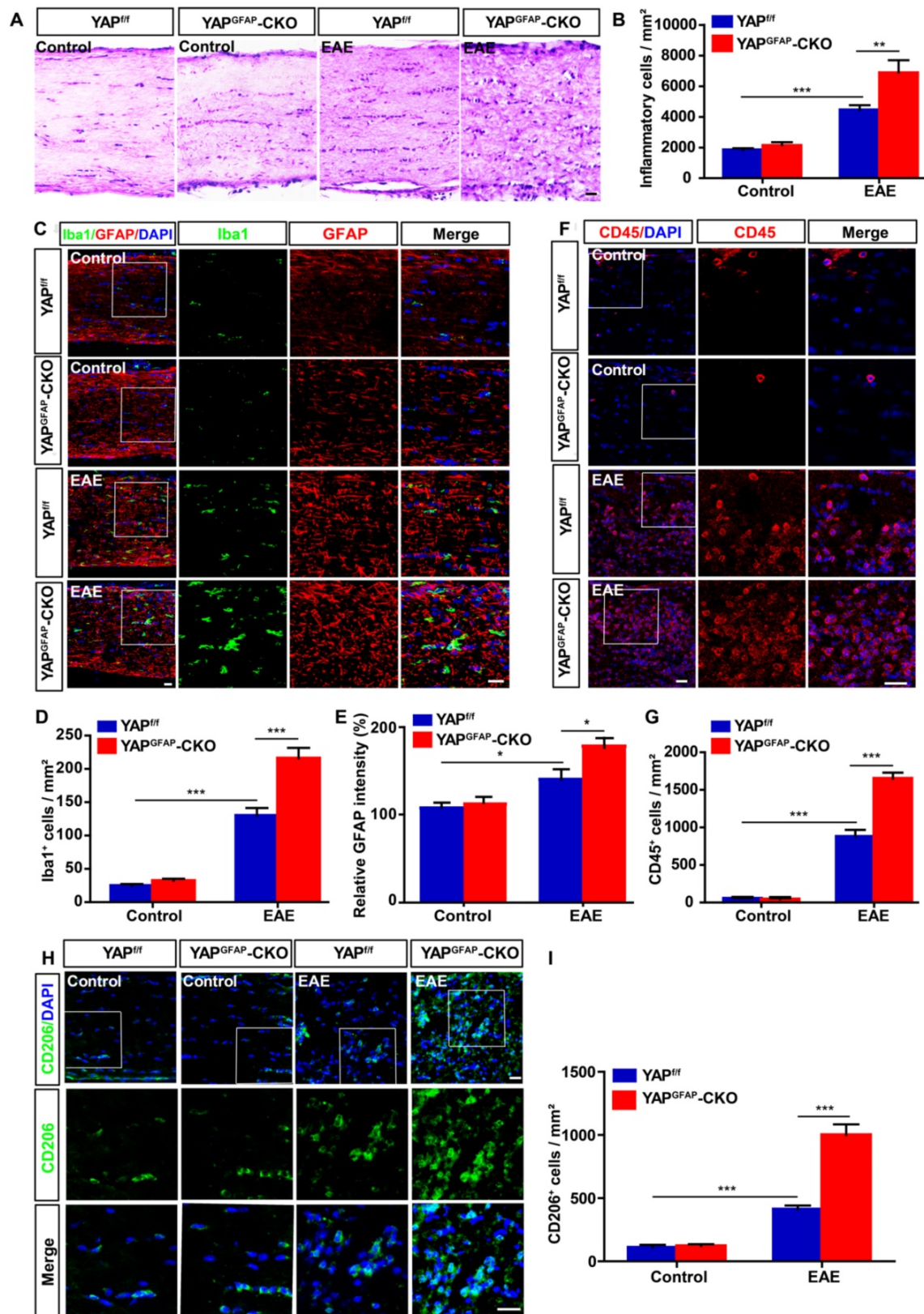


Figure 3. Ablation of YAP in astrocytes exacerbates the inflammatory infiltration in optic nerve of EAE mice. (A) HE staining of optic nerve obtained from YAP^{fl/fl} and YAP^{GFAP-CKO} mice, YAP^{fl/fl} EAE and YAP^{GFAP-CKO} EAE mice. (B) Quantitative analysis of the density of inflammatory cells as shown in (A) (n = 10 per group). (C) Double immunostaining of Iba1 (green) and GFAP (red) in the optic nerve obtained from YAP^{fl/fl} and YAP^{GFAP-CKO} mice, YAP^{fl/fl} EAE and YAP^{GFAP-CKO} EAE mice. (D) Quantitative analysis of the density of Iba1⁺ cells as shown in (C) (n = 12 per group). (E) Quantitative analysis of the relative GFAP intensity as shown in (C) (n = 9 per group, normalized to control). (F) Immunostaining of CD45 (red) in the optic nerve obtained from YAP^{fl/fl} and YAP^{GFAP-CKO} mice, YAP^{fl/fl} EAE and YAP^{GFAP-CKO} EAE mice. (G) Quantitative analysis of the density of CD45⁺ cells as shown in (F) (n = 9 per group). (H) Immunostaining of CD206 (green) in the optic nerve obtained from YAP^{fl/fl} and YAP^{GFAP-CKO} mice, YAP^{fl/fl} EAE and YAP^{GFAP-CKO} EAE mice. (I) Quantitative analysis of the density of CD206⁺ cells as shown in (H) (n = 10 per group). Images of selected regions (white squares) were shown at higher magnification. Data were mean ± SEM, two-way ANOVA with Bonferroni's post-tests, compared with YAP^{fl/fl} group, *P < 0.05, **P < 0.01, ***P < 0.001. Scale bars, 20 μm.

Conditional knockout of YAP in astrocytes exacerbates the inflammatory infiltration in optic nerve of EAE mice

Recent studies have suggested that inflammatory infiltration has a tight connection with demyelination in EAE mice [48, 49]. Thus, HE staining was performed to examine the inflammatory infiltration of optic nerve in EAE mice. As shown in Figure 3A-B, inflammatory infiltration in optic nerve of YAP^{GFAP}-CKO EAE mice was aggravated obviously, compared with that in YAP^{f/f} EAE mice. As inflammatory cells under optic neuritis conditions, including microglial cells, astrocytes and T cells [50, 51], GFAP⁺ astrocytes and Iba1⁺ microglia displayed a hypertrophy morphology, and the density of microglia and intensity of GFAP were increased in YAP^{GFAP}-CKO EAE mice, compared with that in YAP^{f/f} EAE mice (Figure 3C-E). These results indicated that astrocytes and microglia were activated in YAP^{GFAP}-CKO EAE mice. CD45⁺ (a marker of T cells) cells and CD206⁺ (a marker of microglia) cells were also increased in optic nerve of YAP^{GFAP}-CKO EAE mice (Figure 3F-I), suggesting that YAP deletion in astrocytes not only enhanced astrocytic and microglial activation, but also increased the number of microglia and T cells in optic nerve of EAE mice. Next, we performed qPCR experiments to explore expression patterns of chemokines and cytokines in YAP deficient astrocytes of the optic nerve. Results showed Ccl8 and Ccl9 were upregulated in the optic nerve of YAP^{GFAP}-CKO EAE mice, compared with that in YAP^{f/f} EAE mice (Supplementary Figure S4A-B). Additionally, cytokines, including TNF- α and IL-1 β , were also upregulated in optic nerve of YAP^{GFAP}-CKO EAE mice (Supplementary Figure S4C-D). Therefore, we speculated that increase of Ccl8, Ccl9, IL-1 β and TNF- α from YAP-deleted astrocytes may promote activation of microglia and neuroinflammation. Taken together, these results indicate that conditional knockout of YAP in astrocytes aggravates severe inflammatory infiltration in the optic nerve of EAE mice.

Since YAP is involved in proliferation of various cells, such as astrocytes, glioma cells and olfactory ensheathing cells [39, 43, 52], to further explore whether the inflammatory infiltration in YAP^{GFAP}-CKO mice was caused by the proliferation of astrocytes and microglia, double immunostaining of Ki67/GFAP, PH3/GFAP, Ki67/Iba1, and PH3/Iba1 (Ki67 and PH3, cell markers of proliferation) were performed in optic nerve of YAP^{f/f} EAE and YAP^{GFAP}-CKO EAE mice. As shown in Figure 4A-D, the proliferation of astrocytes was decreased in optic nerve of YAP^{GFAP}-CKO EAE mice, compared with that

in YAP^{f/f} EAE mice. However, the proliferation of microglia in optic nerve of YAP^{GFAP}-CKO EAE mice was increased than that in YAP^{f/f} EAE mice (Figure 4E-H), which might be due to the increase of Ccl8, Ccl9, IL-1 β and TNF- α (Supplementary Figure S4A-D). These results suggest that YAP knockout in astrocytes inhibits the proliferation of astrocytes, but promotes the proliferation of microglia in optic nerve of EAE mice.

Conditional knockout of YAP in astrocytes aggravates the inflammatory infiltration and induces more RGCs loss in retina of EAE mice

Inflammatory infiltration in optic neuritis is found not only in optic nerve, but also in retina [51]. As expected, immunostaining showed that there was a significant increase in the density of Iba1⁺ cells and the intensity of GFAP⁺ or vimentin⁺ (a marker of reactive astrocytes) in retina of YAP^{GFAP}-CKO EAE mice, compared with that in YAP^{f/f} EAE mice (Figure 5A-F). Recent studies have found that inflammatory infiltration in optic neuritis is associated with RGCs loss to some extent [53]. To further test this possibility, Nissl staining showed that the density of RGCs in retina of YAP^{GFAP}-CKO EAE mice was indeed significantly decreased (Figure 5G, K), compared with that in YAP^{f/f} EAE mice. Consistently, as shown in Figure 5H-I, the densities of RBPMS⁺ and NeuN⁺ cells (both RBPMS and NeuN are markers of RGCs) were also significantly decreased in retina of YAP^{GFAP}-CKO EAE mice, compared with that in YAP^{f/f} EAE mice (Figure 5L-M). Furthermore, TUNEL staining showed that the apoptosis of RGCs was significantly increased in retina of YAP^{GFAP}-CKO EAE mice (Figure 5J, N). Taken together, these results suggest that conditional knockout YAP in astrocytes aggravates the inflammatory infiltration in retina, which may lead to more RGCs loss in retina of EAE mice.

Downregulation of astrocytic TGF- β signaling pathway may cause more severe neuroinflammation in optic nerve of YAP^{GFAP}-CKO EAE mice

How does YAP regulate the neuroinflammation in MS-ON? To address this question, mRNA sequencing of YAP^{+/+} and YAP^{-/-} astrocytes was performed. GSEA was implemented with all expressed genes on account of hallmark gene set. The results showed that YAP was functionally related to Hedgehog signaling and TGF- β signaling (Figure 6A). Among these, TGF- β signaling has been reported to be highly associated with inflammation [30] and enrichment plot showed that TGF- β 1 was markedly downregulated in YAP^{-/-} astrocytes, compared with that in YAP^{+/+} astrocytes (Figure 6B). To investigate

each gene that was enriched in TGF- β signaling gene set, hierarchical clustering analysis was performed for 49 genes of YAP^{+/+} and YAP^{-/-} groups. The gene expression was evidently different in two groups by

Tree View (Figure 6C). In addition, similar conclusions were obtained from GSVA (Figure 6D) and TGF- β signaling was common to top 3 gene sets of GSEA and GSVA both.

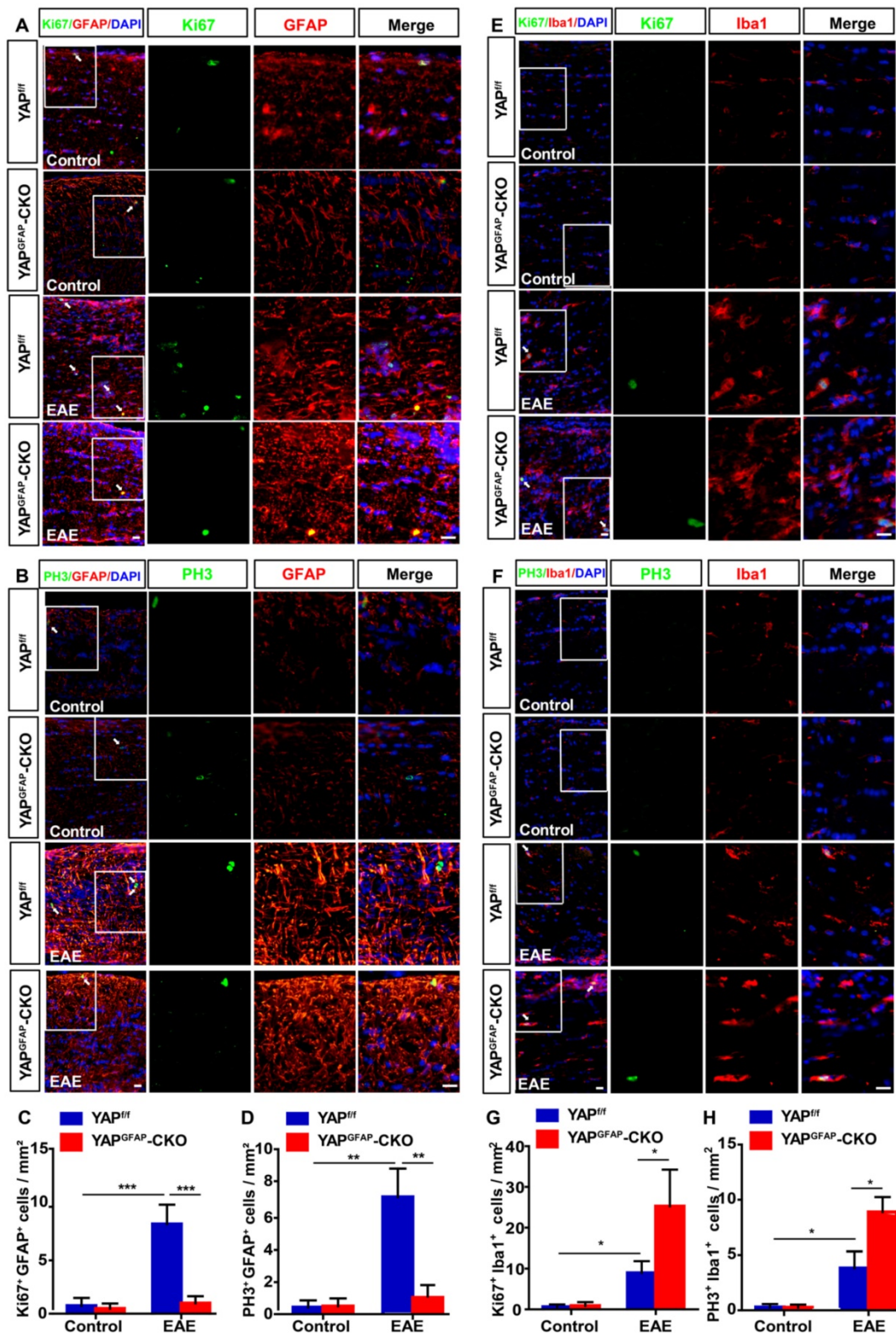


Figure 4. Ablation of YAP in astrocytes inhibits the proliferation of astrocytes and promotes the proliferation of microglia in optic nerve of EAE mice. (A-B) Double immunostaining of Ki67 (green) and GFAP (red) (A) or PH3 (green) and GFAP (red) (B) in the optic nerve of YAP^{fl/fl} and YAP^{GFAP-CKO} mice, YAP^{fl/fl} EAE and YAP^{GFAP-CKO} EAE mice. (C-D) Quantitative analysis of density of Ki67⁺/GFAP⁺ (C) or PH3⁺/GFAP⁺ (D) cells as shown in (A-B) (n = 7 per group). (E-F) Double immunostaining

of Ki67 (green) and Iba1 (red) (E), or PH3 (green) and Iba1 (red) (F) in the optic nerve of YAP^{fl/fl} and YAP^{GFAP-CKO} mice, YAP^{fl/fl} EAE and YAP^{GFAP-CKO} EAE mice. (G-H) Quantitative analysis of the density of Ki67⁺/Iba1⁺ (G) or PH3⁺/Iba1⁺ (H) cells as shown in (E-F) (n = 10 per group). Images of selected regions (white squares) were shown at higher magnification. Data were mean ± SEM, two-way ANOVA with Bonferroni's post-tests, compared with YAP^{fl/fl} group, *P < 0.05, **P < 0.01, ***P < 0.001. Scale bars, 20 μm.

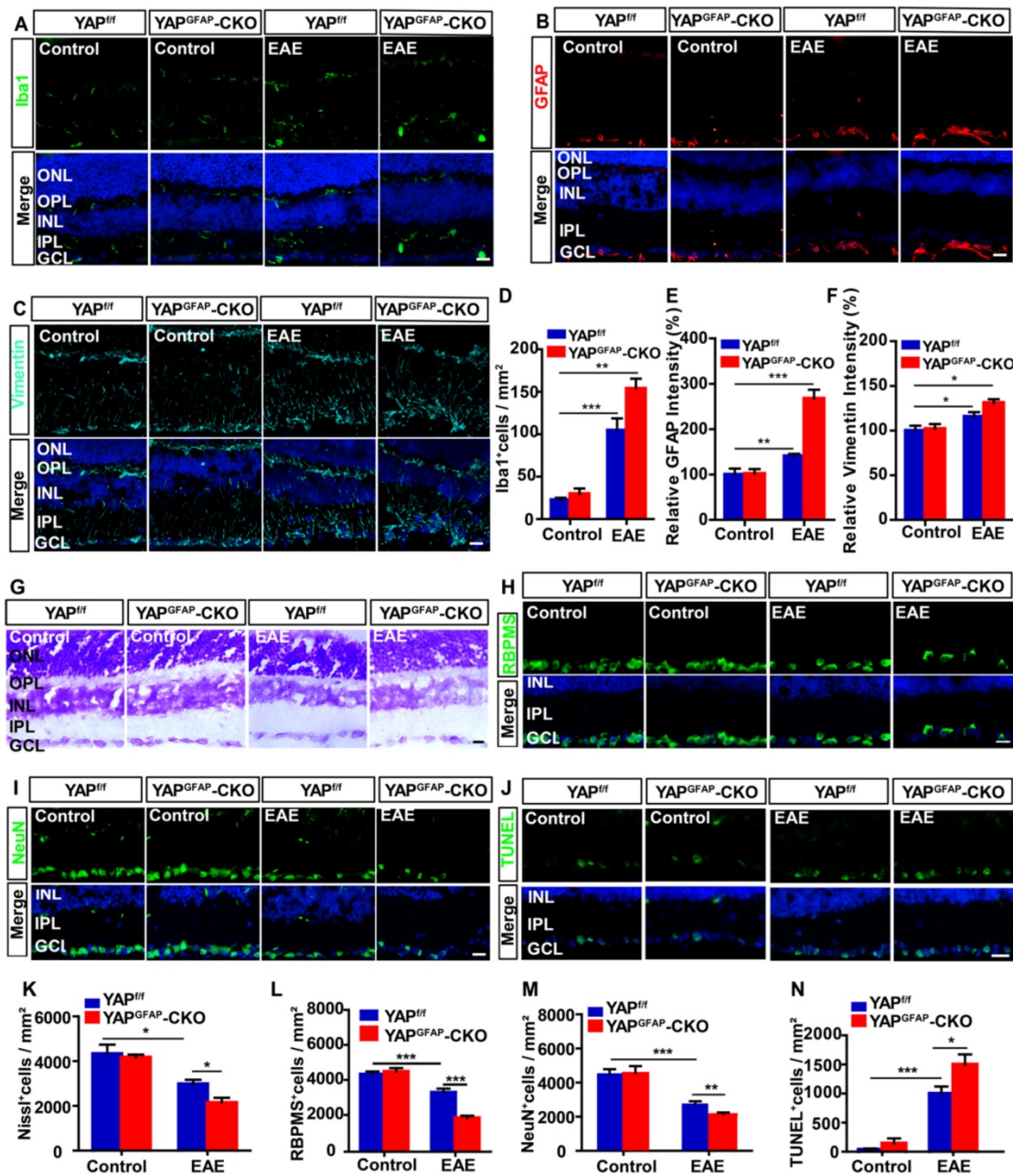


Figure 5. Ablation of YAP in astrocytes exacerbates the inflammation and induces the apoptosis in retina of EAE mice. (A-C) Immunostaining of Iba1 (green) (A), GFAP (red) (B) or Vimentin (cyan) (C) in the retina of YAP^{fl/fl} and YAP^{GFAP-CKO} mice, YAP^{fl/fl} EAE and YAP^{GFAP-CKO} EAE mice. (D) Quantitative analysis of the density of Iba1⁺ cells as shown in (A) (n = 7 per group). (E-F) Quantitative analysis of the relative GFAP intensity (E) or Vimentin intensity (F) as shown in (B-C) (n = 8 per group, normalized to control). (G) Representative images of Nissl staining in the retina of YAP^{fl/fl} and YAP^{GFAP-CKO} mice, YAP^{fl/fl} EAE and YAP^{GFAP-CKO} EAE mice. (H-I) Immunostaining of RBPMs (green) (H) or NeuN (green) (I) in the retina of YAP^{fl/fl} and YAP^{GFAP-CKO} mice, YAP^{fl/fl} EAE and YAP^{GFAP-CKO} EAE mice. (J) Immunostaining analysis of cell apoptosis by TUNEL staining in the retina of YAP^{fl/fl} and YAP^{GFAP-CKO} mice, YAP^{fl/fl} EAE and YAP^{GFAP-CKO} EAE mice. (K) Quantitative analysis of the density of Nissl⁺ cells as shown in (G) (n = 11 per group). (L-M) Quantitative analysis of the density of RBPMs⁺ cells (L) or NeuN⁺ cells (M) as shown in (H-I) (n = 7 per group). (N) Quantitative analysis of the density of TUNEL⁺ cells as shown in (J) (n = 9 per group). Data were mean ± SEM, two-way ANOVA with Bonferroni's post-tests, compared with YAP^{fl/fl} group, *P < 0.05, **P < 0.01, ***P < 0.001. Scale bars, 20 μm.

To confirm the results of bio-informatics analysis, qPCR analysis was performed in YAP^{+/+} and YAP^{-/-} astrocytes. The mRNA levels of TGF-β signaling, such as TGF-β1, Smad1 and Smad3 were markedly decreased in YAP^{-/-} astrocytes, compared with that in YAP^{+/+} astrocytes (Supplementary Figure

S5A), which suggested YAP deletion in astrocytes might down-regulate TGF-β signaling pathway *in vitro*. Additionally, double-immunostaining of TGF-β1 and GFAP showed that the expression of astrocytic TGF-β1 was decreased in optic nerve of YAP^{GFAP-CKO} EAE mice, compared with that in

YAP^{fl/fl} EAE mice (Supplementary Figure S5B-C). To further observe the relationship between YAP and TGF-β signaling pathway *in vivo*, TGF-β signaling pathway, including TGF-β1, Smad1, Smad2, Smad3 and Smad4, was evaluated by qPCR and showed that TGF-β signaling was decreased in YAP^{GFAP}-CKO EAE

mice, compared with that in YAP^{fl/fl} EAE mice (Supplementary Figure S5D). These results suggest that YAP deletion in astrocytes may down-regulate TGF-β signaling pathway *in vitro* and *in vivo*, which may result into more severe inflammation in optic nerve of EAE mice.

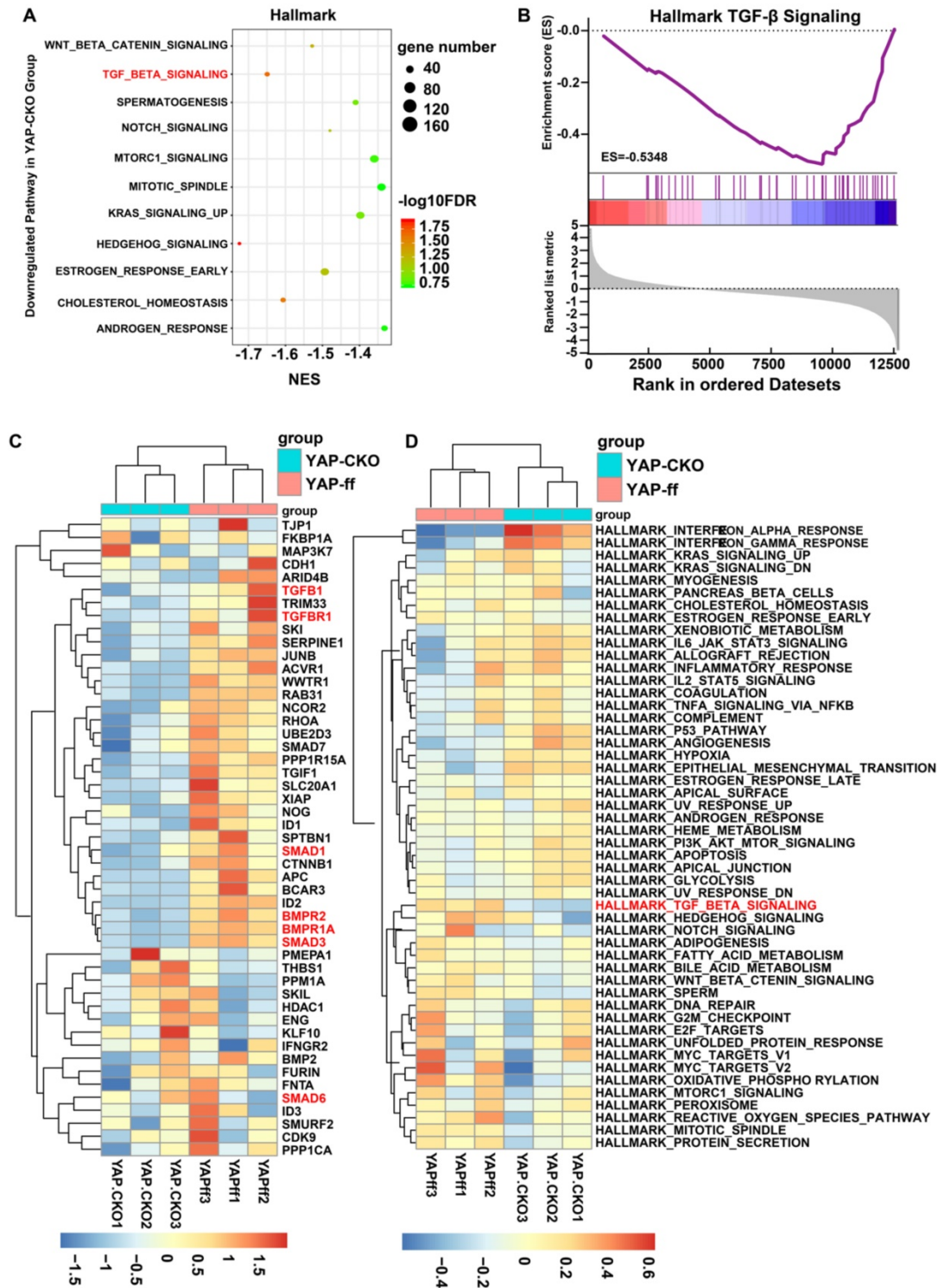


Figure 6. GSEA and GSVA in YAP^{+/+} vs YAP^{-/-} astrocytes based on RNA-seq. (A) The 11 down-regulated gene set with statistically significant (FDR < 0.25). (B) The enrichment plot of TGF-β signaling gene sets. (C) The clustering heatmap of 49 genes in TGF-β signaling gene sets. Red, blue and white respectively represent high expression level, low expression level and no expression difference among the genes. (D) GSVA-derived clustering heatmap of differentially expressed gene sets. Red, blue and white respectively represent high expression level, low expression level and no expression difference among the genes.

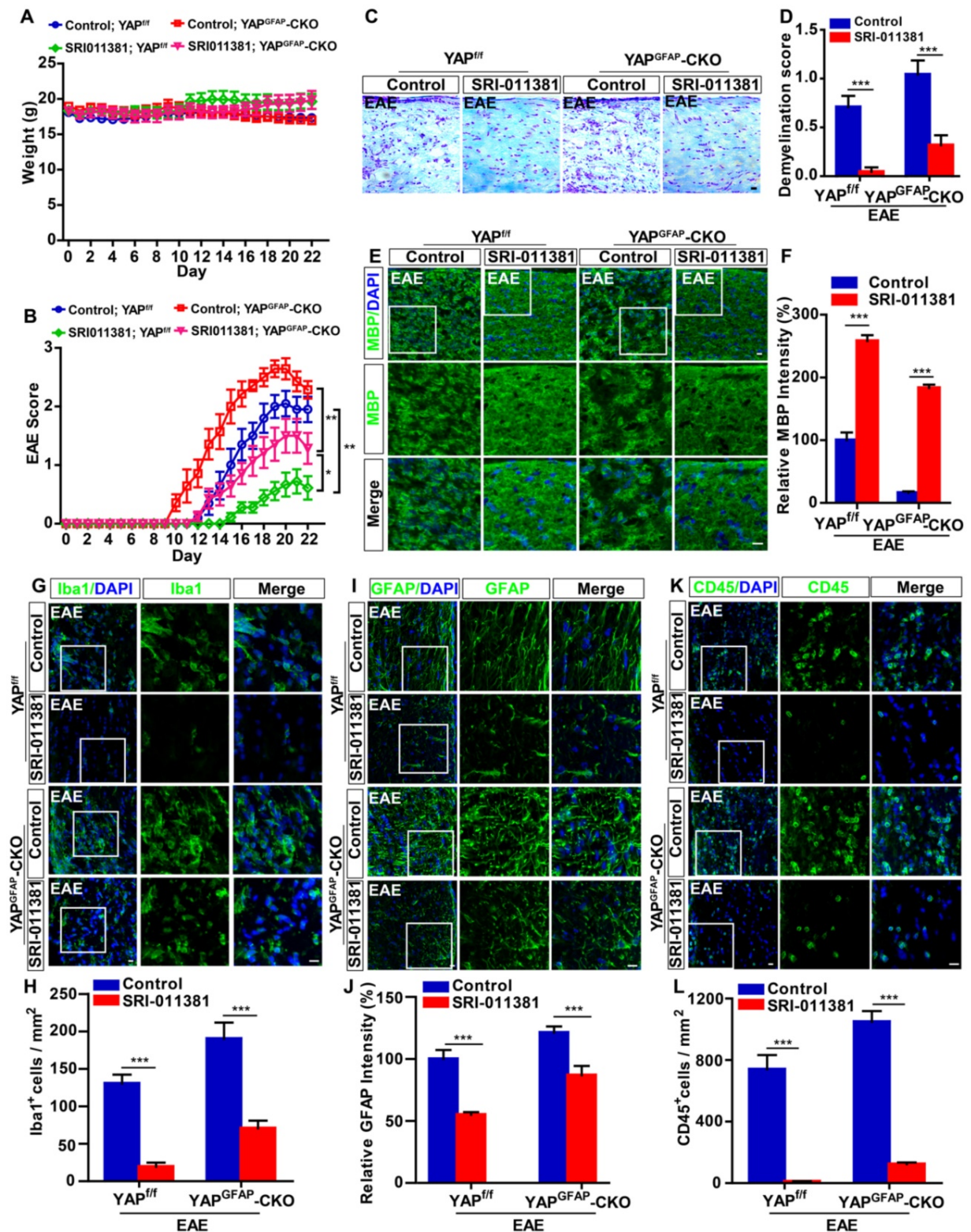


Figure 7. Activation of TGF-β signaling reduces the inflammatory infiltration and demyelination in the optic nerve of EAE mice. (A) The body weight of control-treated YAP^{fl/fl} (n = 10), control-treated YAP^{GFAP-CKO} mice (n = 7), SRI-011381-treated YAP^{fl/fl} (n = 9) and SRI-011381-treated YAP^{GFAP-CKO} mice (n = 8) from 0 to 22 dpi during the process of EAE modeling. (B) The EAE score of control-treated YAP^{fl/fl} mice (n = 10), control-treated YAP^{GFAP-CKO} mice (n = 7), SRI-011381-treated YAP^{fl/fl} mice (n = 9) and SRI-011381-treated YAP^{GFAP-CKO} mice (n = 8) 0 to 22 dpi during the process of EAE modeling. (C) LFB staining in the optic nerve of control-treated YAP^{fl/fl} EAE and YAP^{GFAP-CKO} EAE mice, SRI-011381-treated YAP^{fl/fl} EAE and YAP^{GFAP-CKO} EAE mice. (D) Quantitative analysis of the demyelination score as shown in (C) (n = 7 per group). (E, G, I, K) Immunostaining of MBP (green) (E), Iba1 (green) (G), GFAP (green) (I) or CD45 (green) (K) in the optic nerve of control-treated YAP^{fl/fl} EAE and YAP^{GFAP-CKO} EAE mice, SRI-011381-treated YAP^{fl/fl} EAE and YAP^{GFAP-CKO} EAE mice. (F, J) Quantitative analysis of the relative intensity of MBP (F) or GFAP (J) as shown in (E, I) (n = 6 per group, normalized to control). (H, L) Quantitative analysis of the density of Iba1⁺ cells (H) or CD45⁺ cells (L) as shown in (G, K) (n = 7 per group). Images of selected regions (white squares) were shown at higher magnification. Data were mean ± SEM, two-way ANOVA with Bonferroni's post-tests, compared with control group, *P < 0.05, **P < 0.01, ***P < 0.001. Scale bars, 20 μm.

Activation of TGF- β signaling pathway partially relieves the neuroinflammation and demyelination in optic nerve and retina of YAP^{GFAP}-CKO EAE mice

To further investigate the relationship of YAP and TGF- β 1 in optic neuritis, YAP^{GFAP}-CKO mice and their littermate control YAP^{f/f} mice were performed with intraperitoneally injection of SRI-011381 (an agonist of TGF- β pathway) simultaneously after induction of EAE. As shown in Figure 7A-B, results revealed no significant differences in body weight between SRI-011381 treatment YAP^{f/f} and YAP^{GFAP}-CKO mice during the process of EAE modeling (Figure 7A). However, SRI-011381 treatment significantly reduced the clinical scores in YAP^{GFAP}-CKO EAE mice, compared with control-treated YAP^{GFAP}-CKO EAE mice (Figure 7B). Moreover, HE and Nissl staining revealed that SRI-011381 treatment significantly inhibited inflammatory infiltration and relieved the loss of neurons in YAP^{GFAP}-CKO EAE mice (Supplementary Figure S6A-B).

Additionally, SRI-011381 treatment relieved the demyelination in optic nerve of YAP^{f/f} EAE mice and YAP^{GFAP}-CKO EAE mice, compared with that in control mice (Figure 7C-F). However, the demyelination degree of SRI-011381-treated YAP^{GFAP}-CKO EAE mice was more severe than that of SRI-011381-treated YAP^{f/f} EAE mice (Figure 7 C-F). As shown in Figure 7G-L, immunostaining of Iba1, GFAP and CD45 also indicated that the obvious inflammatory infiltration was ameliorated in optic nerve of YAP^{f/f} EAE and YAP^{GFAP}-CKO EAE mice treated with SRI-011381. Interestingly, immunostaining of Iba1 and GFAP in retina also suggested that the SRI-011381 treatment did suppress the inflammatory infiltration (Supplementary Figure S6C-F) and rescue RGCs loss (Supplementary Figure S6G-H) in retina of YAP^{GFAP}-CKO EAE mice. Taken together, these results indicate that activation of TGF- β signaling pathway partially relieves the neuroinflammation and demyelination in optic nerve and retina of YAP^{GFAP}-CKO EAE mice.

Activation of YAP signaling relieves the neuroinflammatory infiltration and demyelination in optic nerve, and reduces loss of RGCs in retina of EAE mice

Recent studies showed that XMU-MP-1 can activate YAP by inhibiting MST1 and MST2 of Hippo signaling pathway, which is reported to promote regeneration in the liver and spinal cord injury (SCI) [43, 54], and protect the heart [55] and brain [56]. As expected, immunohistochemistry and immunostaining showed that XMU-MP-1 treatment indeed

significantly activated YAP in optic nerve astrocytes of mice (Supplementary Figure S7A-D). As shown in Figure 8A, there was no significant difference in the body weight between control and XMU-MP-1-treated mice during the process of EAE, however, XMU-MP-1 treatment significantly reduced the clinical scores (Figure 8B).

Then, the gross morphology of optic nerve and retina was observed by HE and Nissl staining and showed that XMU-MP-1 treatment significantly relieved the damage in optic nerve (Figure 8C-D). LFB staining and immunostaining of MBP showed that, the demyelination in optic nerve was relieved in the XMU-MP-1-treated EAE mice, compared with that in control-treated EAE mice (Figure 8E-H). As shown in Figure 8I-N, immunostaining of Iba1, GFAP and CD45 also indicated that XMU-MP-1 treatment did ameliorate the inflammatory infiltration in optic nerve. As expected, the inflammatory infiltration was significantly decreased in retina of XMU-MP-1-treated EAE mice (Figure 8O-R). Meanwhile, XMU-MP-1 treatment also reduced the loss of RGCs in retina of EAE mice (Figure 8S-T). Furthermore, results from qPCR showed that XMU-MP-1 treatment upregulated TGF- β signaling in optic nerve of EAE mice (Supplementary Figure S5E), which was consistent with the findings from our bio-informatics analysis. Taken together, these results indicated that activation of YAP signaling by XMU-MP-1 could reduce inflammatory infiltration and demyelination and the loss of RGCs in EAE mice through upregulating the TGF- β signaling.

Discussion

In this study, we provide evidence of astrocytic YAP's function in the neuroinflammation and demyelination of optic neuritis. YAP prevents the neuroinflammation and demyelination in optic nerve and retina of EAE mice through upregulation of TGF- β signaling pathway (Figure 9).

The characteristically pathological changes of EAE are multiple demyelinating plaques, reactive glial hyperplasia and axonal damage [57]. The mammalian optic nerve contains three types of optic glial cells, including oligodendrocytes, microglia and astrocytes [51, 58]. Previous researches have paid much more attention to microglia, immune cells and oligodendrocytes in EAE [59, 60]. Nevertheless, recent accumulating evidences suggest that astrocytes are also key regulatory cells for CNS neuroinflammation in MS/EAE [12, 61]. Reactive astrogliosis is a prominent feature of the chronic and widespread adaptive immune inflammation of CNS that occurs during conditions such as EAE and MS, and the basic process of reactive astrogliosis has long been regarded

as primarily detrimental in MS and EAE [62, 63]. Several studies have pointed out that perforin can be expressed by reactive astrocytes in MS, which represents the ongoing inflammation of nerves [64]. Ablation of proliferating reactive astrocytes increased the spread of infiltrating inflammatory cells and the

exacerbation of EAE clinical signs [13]. Consistent with previous studies, our results in this study revealed that astrocytes were activated in optic nerve of EAE (Supplementary Figure S1). But the mechanism underlying in MS-ON that regulated by astrocytes remains unclear.

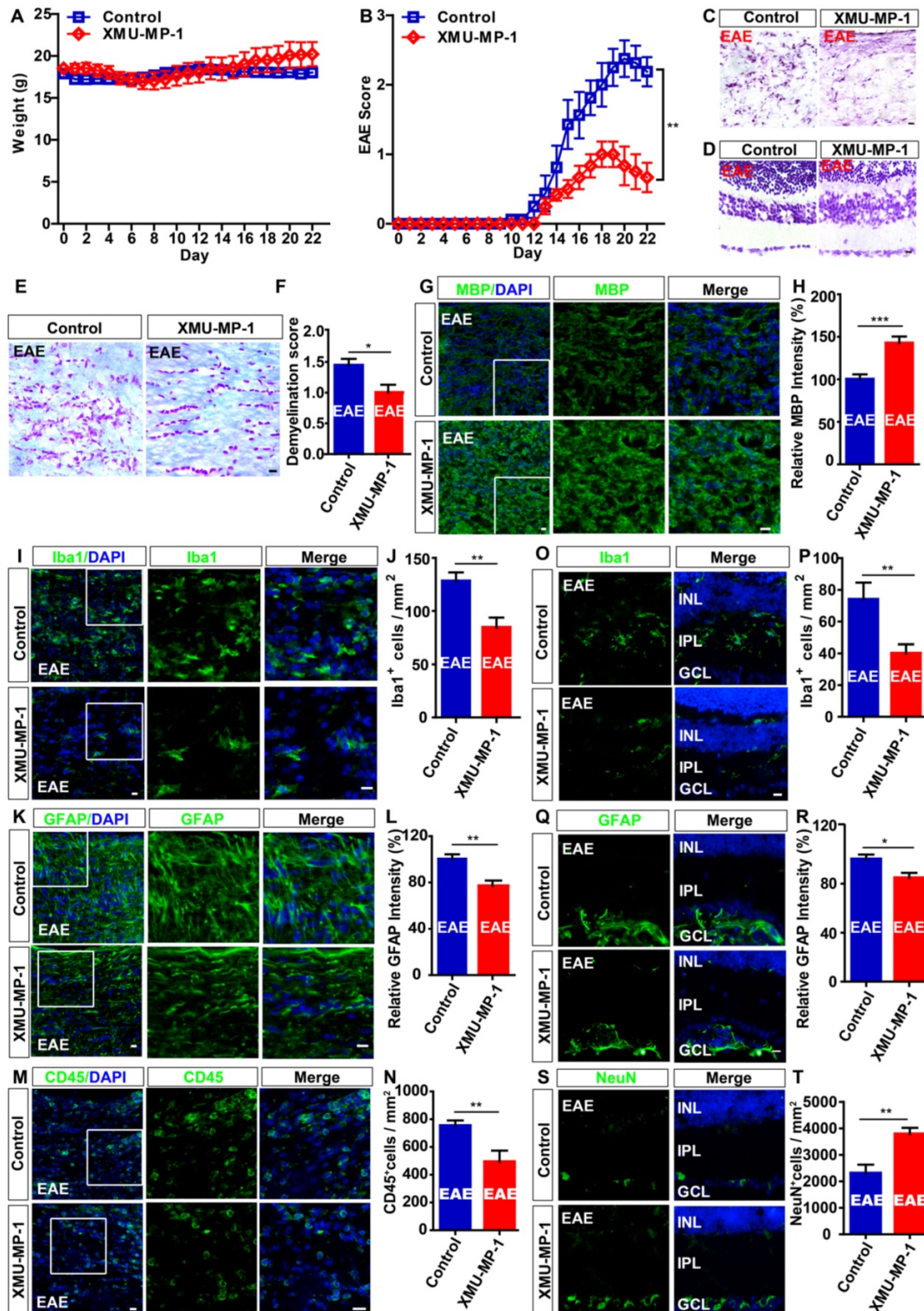


Figure 8. Activation of YAP signaling by XMU-MP-1 partially reduces the inflammation and demyelination of optic nerve, and the loss of RGCs in EAE mice. (A) The body weight of control (n = 8) and XMU-MP-1 (n = 6) treatment EAE mice from 0 to 22 dpi during EAE modeling (two-way ANOVA with Bonferroni's post-tests).

(B) The EAE score of control (n = 8) and XMU-MP-1 (n = 6) treatment EAE mice 0 to 22 dpi during the process of EAE modeling (two-way ANOVA with Bonferroni's post-tests). (C) HE staining of optic nerve obtained from control and XMU-MP-1-treated EAE mice. (D) Nissl staining of retina obtained from control and XMU-MP-1-treated EAE mice. (E) LFB staining of optic nerve obtained from control and XMU-MP-1-treated EAE mice. (F) Quantitative analysis of the demyelination score of control and XMU-MP-1-treated EAE mice as shown in (E) (n = 7 per group, Student's t-test). (G, I, K, M) Immunostaining of MBP (green) (G), Iba1 (green) (I), GFAP (green) (K) or CD45 (green) (M) in the optic nerve of control and XMU-MP-1-treated EAE mice. (H, L) Quantitative analysis of the relative MBP intensity (H) or GFAP intensity (L) as shown in (G, K) (n = 7 per group, normalized to control, Student's t-test). (J, N) Quantitative analysis of the density of Iba1⁺ cells (J) or CD45⁺ cells (N) as shown in (I, M) (n = 6 per group, Student's t-test). (O, Q, S) Immunostaining of Iba1 (green) (O), GFAP (green) (Q) or NeuN (green) (S) in the retina of control and XMU-MP-1-treated EAE mice. (P, T) Quantitative analysis of the density of Iba1⁺ cells (P) or NeuN⁺ cells (T) as shown in (O, S) (n = 5 per group, Student's t-test). (R) Quantitative analysis of the relative GFAP intensity as shown in (Q) (n = 7 per group, normalized to control, Student's t-test). Images of selected regions (white squares) were shown at higher magnification. Data were mean ± SEM, compared with control group, *P < 0.05, **P < 0.01, ***P < 0.001. Scale bars, 20 μm.

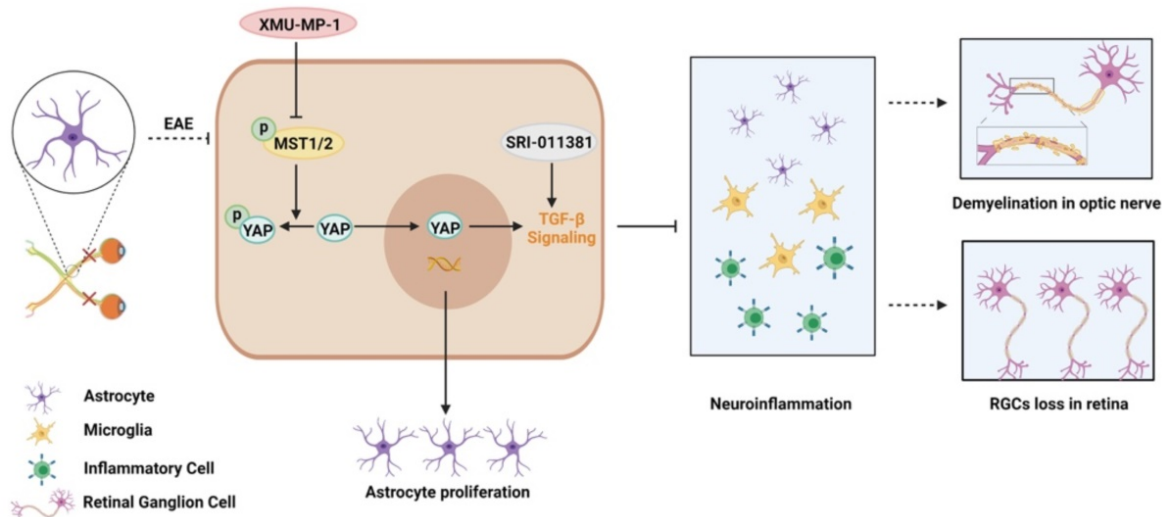


Figure 9. Working model of YAP's functions in protection the optic nerve and retina through TGF-β signaling in an EAE model. YAP signaling is activated in optic nerve astrocytes of EAE mice. Activation of YAP signaling promotes the proliferation of astrocytes, and upregulates TGF-β signaling to prevent the neuroinflammation in optic nerve and retina of EAE mice, which further inhibits the demyelination of optic nerve and the loss of RGCs in retina. XMU-MP-1 is an inhibitor of Hippo kinase MST1/2 to activate YAP signaling. SRI-011381 is an agonist of TGF-β signaling.

YAP acts as a transcriptional co-activator and plays an important role in CNS [65]. Our previous studies have shown that YAP is upregulated and activated in GFAP⁺ astrocytes after SCI [43]. Consistent with our previous studies, we also found that YAP was upregulated and activated in optic nerve astrocytes of EAE mice (Figure 1). However, interestingly, our histological observations revealed that YAP knockout in astrocytes did not affect the visual development (Supplementary Figure S3). Previous studies have shown that deletion of YAP and TAZ may affect development of optic nerve and retina. For example, YAP-deficient retinal progenitors displayed decreased S-phase cells and altered cell cycle progression in the developing mouse eye [66]; activated YAP/TAZ promotes rescuing angiogenesis and barrier genesis in retina [67]. It's probably because GFAP⁺ astrocytes are late to emerge during the embryonic development of optic nerve, and there is virtually no GFAP⁺ astrocytes at E16, and only 8% of the purified cells are GFAP⁺ astrocytes at E17 [68]. Furthermore, astrocytes in optic nerve are actually not activated under physiological conditions [68, 69]. However, in optic neuritis, the deletion of YAP in astrocytes aggravated the demyelination (Figure 2) and inflammatory infiltration (Figure 3) in optic nerve, promoted the activation of astrocytes and

microglia, and induced a drastic increase of RGCs death in retina (Figure 5). The microglia may be activated by some factors secreted by YAP-deleted astrocytes. Studies have shown that the activation of microglia and the neuroinflammation may be excessive effects of the JAK-STAT inflammatory pathway through YAP-deficient astrocytes [21]. In addition, abnormal activation of astrocytes has been associated with upregulation and secretion of cytokines, such as TNF-α and IL-3, as well as chemokines like Ccl3, Ccl4 and Ccl8, which may also attract microglia and increase neuroinflammation [70-72]. Consistent with previous study, we found that increase of Ccl8, Ccl9, TNF-α and IL-1β from YAP-deleted astrocytes might promote activation of microglia and neuroinflammation (Supplementary Figure S4). Taken together, these results indicate that conditional YAP knockout in astrocytes exacerbates inflammatory infiltration in the optic nerve of EAE mice.

How does YAP signaling in astrocytes suppress the neuroinflammation of MS-ON? Astrocytic TGF-β signaling plays multiple functions in protecting against chronic and widespread adaptive immune inflammation of the CNS. For example, inhibiting astrocytic TGF-β signaling was found to aggravate inflammation in the peri-infarct cortex during the

subacute period following distal middle cerebral occlusion [73], and astrocytic TGF- β signaling limits inflammation and reduces neuronal damage during CNS toxoplasma infection [74]. Additionally, astrocytic TGF- β 1 protects synapses against A β oligomers in Alzheimer's disease model [75]. Consistent with these previous studies, we found that downregulation of TGF- β signaling in YAP^{GFAP}-CKO EAE mice promoted neuroinflammation. These results suggest that astrocytic TGF- β signaling has conservative anti-neuroinflammation roles in different disease model. Furthermore, numerous studies have demonstrated that TGF- β is significantly upregulated in MS patients, with its injection into EAE mice models associated with a reduction in frequency and severity of attacks [31-33]. Conversely, lacking TGF- β was found to develop a multifocal inflammatory disease [76], indicating that TGF- β might be playing an important role in MS or EAE. Previous studies have shown that YAP can regulate TGF- β signaling in various situations [35, 77]. For example, increased nuclear YAP/TAZ overcomes TGF- β 1-mediated tumor suppressive functions (e.g. cytostasis) and concomitantly drives tumorigenic transcriptional events by promoting the activity of YAP/TEAD-SMAD complexes in breast cancer cells [78]. In skin wound healing, the knockdown of YAP/TAZ markedly delayed the rate of wound closure and reduced the expression of TGF- β 1, and YAP/TAZ also modulated the expression of TGF- β signaling pathway components such as Smad2, Smad7 and p21 [79]. Consistent with these previous studies, our RNA-seq results showed that TGF- β 1 related signaling, including TGF- β 1, smad1, smad3, BMPR1 and BMPR2 were significantly decreased in YAP^{-/-} groups (Figure 6). To strengthen the links between YAP and TGF- β signaling, TGF- β related signaling pathways in mice, either competent or lacking YAP, administered with XMU-MP-1, was evaluated by qPCR, including TGF- β 1, Smad1, Smad2, Smad3 and Smad4 (Supplementary Figure S5), and the results of qPCR further confirmed the sequencing analysis. Therefore, YAP might act as a positive up-stream regulator of TGF- β 1/Smad signaling, leading to protect the optic nerve and retina against damage in EAE mice. But our previous study showed that TGF- β 1 was upregulated in astrocytes following YAP deletion [21]. This may be due to different model and different assays (PCR array VS RNA-seq). The present study had other evidences to support the hypothesis that astrocytic YAP suppresses neuroinflammation in optic neuritis by upregulating TGF- β 1 signaling. For example, SRI-011381 (an agonist of TGF- β pathway) treatment partially rescued infiltration of CD45⁺ cells and activated microglia in YAP^{GFAP}-CKO EAE mice,

compared with that in control mice. Although we could not exclude the possibility that SRI-011381 affected other cells in EAE mice, we found that TGF- β signaling was downregulated by YAP knockout in astrocytes based on RNA-seq, qPCR and immunostaining (Figure 6 and Supplementary Figure S5). These results suggest that TGF- β signaling may be a downstream of YAP signaling in regulation of neuroinflammation in EAE. However, detailed mechanism how YAP regulates expression of TGF- β 1 in EAE requires further investigation.

To further elucidate YAP's therapeutic effect on recovery of optic neuritis, we treated mice with XMU-MP-1 to activate YAP signaling after EAE induction. Results showed that treatment relieved inflammatory infiltration and demyelination in optic nerve after EAE induction, consistent with our previous study which also has shown that XMU-MP-1 exerts a certain degree of therapeutic effect on SCI [43]. Previous studies have shown that YAP is mainly expressed in astrocytes, but not in microglia and T cells [21, 43]. Consistent with these previous studies, results of the present study showed that YAP was mainly expressed in astrocytes, and not microglial cells (Figure 1). Therefore, XMU-MP-1 treatment mainly affects astrocytes, whereas the responses of CD45⁺ cells or microglia to XMU-MP-1 treatment may be indirect. Taken together, these results suggest that YAP signaling could be a new therapeutic target for treatment of MS-ON.

Conclusions

In summary, these results suggest that YAP may upregulate TGF- β signaling pathway to prevent inflammatory infiltration, demyelination and RGCs death in optic neuritis. These results not only reveal the unrecognized function of YAP signaling in optic neuritis, but also further link YAP with TGF- β 1, which may provide a new potential therapeutic target for optic neuritis in clinic by selectively enhancing the function of YAP-TGF- β signaling pathway.

Abbreviations

BSA: bovine serum albumin; CKO: Conditional knockout; CNS: central nervous system; dpi: day post injection; EAE: experimental autoimmune encephalomyelitis; EM: electron microscopy; GSEA: gene set enrichment analysis; GSVA: gene set variation analysis; HE: Hematoxylin-Eosin; LFB: Luxol Fast Blue; MBP: myelin basic protein; MOG₃₅₋₅₅: myelin oligodendrocyte glycoprotein 35-55; MS: multiple sclerosis; MS-ON: MS related optic neuritis; PBS: phosphate-buffered saline; PFA: paraformaldehyde; qPCR: quantitative real-time PCR; RGCs: retinal ganglion cells; SCI: spinal cord injury; TAZ:

transcriptional coactivator with PDZ-binding motif; TGF- β : transforming growth factor- β ; YAP: yes-associated protein.

Supplementary Material

Supplementary figures.

<http://www.thno.org/v11p8480s1.pdf>

Acknowledgments

We thank Bio-ultrastructure analysis Lab. of Analysis center of Agrobiological and environmental sciences, Zhejiang University.

Ethics approval and consent to participate

All surgical procedures and experimental protocols were approved by the Animal Care and Use Committee of Wenzhou Medical University in Wenzhou (IACUC no: 2018-242).

Availability of data and materials

The data sets used and analyzed during the current study are available from the corresponding author on reasonable request.

Funding

This work was supported by the Natural Science Foundation of Zhejiang Province (grant numbers LR18C090001 and LR21H090001); National Natural Science Foundation (grant numbers 92049104, 81971142 and 81971172); Shenzhen-Hong Kong Institute of Brain Science-Shenzhen Fundamental Research Institutions (grant number NYKFKT2019008 and the Research Start-up Project by Hangzhou Normal University (grant number 4125C5021920453); Public Welfare Science and Technology Project of Wenzhou (No. Y20190132); Zhejiang Province Science and Technology Plan Research and Xinmiao Talent Program (grant numbers 2019R413078 and 2020R413077); National College Students Innovation and Entrepreneurship Training Program (grant numbers 20201034039).

Competing Interests

The authors have declared that no competing interest exists.

References

- Voskuhl RR, Itoh N, Tassoni A, Matsukawa MA, Ren E, Tse V, et al. Gene expression in oligodendrocytes during remyelination reveals cholesterol homeostasis as a therapeutic target in multiple sclerosis. *Proc Natl Acad Sci U S A*. 2019; 116: 10130-9.
- Cramer SP, Modvig S, Simonsen HJ, Frederiksen JL, Larsson HB. Permeability of the blood-brain barrier predicts conversion from optic neuritis to multiple sclerosis. *Brain*. 2015; 138: 2571-83.
- Ziemssen T, Wilhelm H, Ziemssen F. [Multiple sclerosis. An update with practical guidelines for ophthalmologists]. *Ophthalmologe*. 2006; 103: 621-41; quiz 42-3.
- Wilmes AT, Reinehr S, Kühn S, Pedreiturria X, Petrikowski L, Faissner S, et al. Laquinimod protects the optic nerve and retina in an experimental autoimmune encephalomyelitis model. *J Neuroinflammation*. 2018; 15: 183.
- Lampert EJ, Andorra M, Torres-Torres R, Ortiz-Pérez S, Llufríu S, Sepúlveda M, et al. Color vision impairment in multiple sclerosis points to retinal ganglion cell damage. *J Neurol*. 2015; 262: 2491-7.
- Brusaferri F, Candelise L. Steroids for multiple sclerosis and optic neuritis: a meta-analysis of randomized controlled clinical trials. *J Neurol*. 2000; 247: 435-42.
- Dietrich M, Helling N, Hilla A, Heskamp A, Issberner A, Hildebrandt T, et al. Early alpha-lipoic acid therapy protects from degeneration of the inner retinal layers and vision loss in an experimental autoimmune encephalomyelitis-optic neuritis model. *J Neuroinflammation*. 2018; 15: 71.
- Brosnan C, Raine C. The astrocyte in multiple sclerosis revisited. *Glia*. 2013; 61: 453-65.
- Brambilla R, Dvorianchikova G, Barakat D, Ivanov D, Bethea J, Shestopalov V. Transgenic inhibition of astroglial NF- κ B protects from optic nerve damage and retinal ganglion cell loss in experimental optic neuritis. *J Neuroinflammation*. 2012; 9: 213.
- Pittock SJ, Berthele A, Fujihara K, Kim HJ, Levy M, Palace J, et al. Eculizumab in Aquaporin-4-Positive Neuromyelitis Optica Spectrum Disorder. *N Engl J Med*. 2019; 381: 614-25.
- Duan T, Verkman AS. Experimental animal models of aquaporin-4-IgG-seropositive neuromyelitis optica spectrum disorders: progress and shortcomings. *Brain Pathol*. 2020; 30: 13-25.
- Itoh N, Itoh Y, Tassoni A, Ren E, Kaito M, Ohno A, et al. Cell-specific and region-specific transcriptomics in the multiple sclerosis model: Focus on astrocytes. *Proc Natl Acad Sci U S A*. 2018; 115: E302-e9.
- Voskuhl RR, Peterson RS, Song B, Ao Y, Morales LB, Tiwari-Woodruff S, et al. Reactive astrocytes form scar-like perivascular barriers to leukocytes during adaptive immune inflammation of the CNS. *J Neurosci*. 2009; 29: 11511-22.
- Zamora NN, Cheli VT, Santiago González DA, Wan R, Paez PM. Deletion of Voltage-Gated Calcium Channels in Astrocytes during Demyelination Reduces Brain Inflammation and Promotes Myelin Regeneration in Mice. *J Neurosci*. 2020; 40: 3332-47.
- Camargo FD, Gokhale S, Johnnidis JB, Fu D, Bell GW, Jaenisch R, et al. YAP1 increases organ size and expands undifferentiated progenitor cells. *Curr Biol*. 2007; 17: 2054-60.
- Piccolo S, Dupont S, Cordenonsi M. The biology of YAP/TAZ: hippo signaling and beyond. *Physiol Rev*. 2014; 94: 1287-312.
- Beverdam A, Claxton C, Zhang X, James G, Harvey KF, Key B. Yap controls stem/progenitor cell proliferation in the mouse postnatal epidermis. *J Invest Dermatol*. 2013; 133: 1497-505.
- Yu FX, Zhao B, Guan KL. Hippo Pathway in Organ Size Control, Tissue Homeostasis, and Cancer. *Cell*. 2015; 163: 811-28.
- Huang Z, Hu J, Pan J, Wang Y, Hu G, Zhou J, et al. YAP stabilizes SMAD1 and promotes BMP2-induced neocortical astrocytic differentiation. *Development*. 2016; 143: 2398-409.
- Huang Z, Sun D, Hu JX, Tang FL, Lee DH, Wang Y, et al. Neogenin Promotes BMP2 Activation of YAP and Smad1 and Enhances Astrocytic Differentiation in Developing Mouse Neocortex. *J Neurosci*. 2016; 36: 5833-49.
- Huang Z, Wang Y, Hu G, Zhou J, Mei L, Xiong WC. YAP Is a Critical Inducer of SOCS3, Preventing Reactive Astroglia. *Cereb Cortex*. 2016; 26: 2299-310.
- Grove M, Kim H, Santerre M, Krupka AJ, Han SB, Zhai J, et al. YAP/TAZ initiate and maintain Schwann cell myelination. *Elife*. 2017; 6.
- Yu H, Cao X, Li W, Liu P, Zhao Y, Song L, et al. Targeting connexin 43 provides anti-inflammatory effects after intracerebral hemorrhage injury by regulating YAP signaling. *J Neuroinflammation*. 2020; 17: 322.
- Kitagawa M. A Sveinsson's chorioretinal atrophy-associated missense mutation in mouse Tead1 affects its interaction with the co-factors YAP and TAZ. *Biochem Biophys Res Commun*. 2007; 361: 1022-6.
- Matsumoto H, Murakami Y, Kataoka K, Lin H, Connor KM, Miller JW, et al. Mammalian STE20-like kinase 2, not kinase 1, mediates photoreceptor cell death during retinal detachment. *Cell Death Dis*. 2014; 5: e1269.
- Raghunathan VK, Morgan JT, Dreier B, Reilly CM, Thomasy SM, Wood JA, et al. Role of substratum stiffness in modulating genes associated with extracellular matrix and mechanotransducers YAP and TAZ. *Invest Ophthalmol Vis Sci*. 2013; 54: 378-86.
- Lund H, Pieber M, Parsa R, Grommisch D, Ewing E, Kular L, et al. Fatal demyelinating disease is induced by monocyte-derived macrophages in the absence of TGF- β signaling. *Nat Immunol*. 2018; 19: 1-7.
- Qin Y, Garrison BS, Ma W, Wang R, Jiang A, Li J, et al. A Milieu Molecule for TGF- β Required for Microglia Function in the Nervous System. *Cell*. 2018; 174: 156-71.e16.
- Luo J, Ho PP, Buckwalter MS, Hsu T, Lee LY, Zhang H, et al. Glia-dependent TGF-beta signaling, acting independently of the TH17

- pathway, is critical for initiation of murine autoimmune encephalomyelitis. *J Clin Invest.* 2007; 117: 3306-15.
30. Tan YV, Abad C, Lopez R, Dong H, Liu S, Lee A, et al. Pituitary adenyl cyclase-activating polypeptide is an intrinsic regulator of Treg abundance and protects against experimental autoimmune encephalomyelitis. *Proc Natl Acad Sci U S A.* 2009; 106: 2012-7.
 31. Lee PW, Severin ME, Lovett-Racke AE. TGF- β regulation of encephalitogenic and regulatory T cells in multiple sclerosis. *Eur J Immunol.* 2017; 47: 446-53.
 32. Matejuk A, Dwyer J, Hopke C, Vandenbark AA, Offner H. Opposing roles for TGF-beta1 and TGF-beta3 isoforms in experimental autoimmune encephalomyelitis. *Cytokine.* 2004; 25: 45-51.
 33. Santambrogio L, Hochwald GM, Saxena B, Leu CH, Martz JE, Carlino JA, et al. Studies on the mechanisms by which transforming growth factor-beta (TGF-beta) protects against allergic encephalomyelitis. Antagonism between TGF-beta and tumor necrosis factor. *J Immunol.* 1993; 151: 1116-27.
 34. Cui X, Morales RT, Qian W, Wang H, Gagner JP, Dolgalev I, et al. Hacking macrophage-associated immunosuppression for regulating glioblastoma angiogenesis. *Biomaterials.* 2018; 161: 164-78.
 35. Piersma B, Bank RA, Boersema M. Signaling in Fibrosis: TGF- β , WNT, and YAP/TAZ Converge. *Front Med (Lausanne).* 2015; 2: 59.
 36. Yu HX, Yao Y, Bu FT, Chen Y, Wu YT, Yang Y, et al. Blockade of YAP alleviates hepatic fibrosis through accelerating apoptosis and reversion of activated hepatic stellate cells. *Mol Immunol.* 2019; 107: 29-40.
 37. Milenkovic U, Ilg MM, Zuccato C, Ramazani Y, De Ridder D, Albersen M. Simvastatin and the Rho-kinase inhibitor Y-27632 prevent myofibroblast transformation in Peyronie's disease-derived fibroblasts via inhibition of YAP/TAZ nuclear translocation. *BJU Int.* 2019; 123: 703-15.
 38. Liu Y, He K, Hu Y, Guo X, Wang D, Shi W, et al. YAP modulates TGF- β 1-induced simultaneous apoptosis and EMT through upregulation of the EGF receptor. *Sci Rep.* 2017; 7: 45523.
 39. Bao X, Xu X, Wu Q, Zhang J, Feng W, Yang D, et al. Sphingosine 1-phosphate promotes the proliferation of olfactory ensheathing cells through YAP signaling and participates in the formation of olfactory nerve layer. *Glia.* 2020; 68: 1757-74.
 40. Li Q, Powell N, Zhang H, Belevych N, Ching S, Chen Q, et al. Endothelial IL-1R1 is a critical mediator of EAE pathogenesis. *Brain Behav Immun.* 2011; 25: 160-7.
 41. Herges K, de Jong BA, Kolkowitz I, Dunn C, Mandelbaum G, Ko RM, et al. Protective effect of an elastase inhibitor in a neuromyelitis optica-like disease driven by a peptide of myelin oligodendroglial glycoprotein. *Mult Scler.* 2012; 18: 398-408.
 42. Liu Y, Gao L, Zhao X, Guo S, Liu Y, Li R, et al. Saikosaponin A Protects From Pressure Overload-Induced Cardiac Fibrosis via Inhibiting Fibroblast Activation or Endothelial Cell EndMT. *Int J Biol Sci.* 2018; 14: 1923-34.
 43. Xie C, Shen X, Xu X, Liu H, Li F, Lu S, et al. Astrocytic YAP Promotes the Formation of Glia Scars and Neural Regeneration after Spinal Cord Injury. *J Neurosci.* 2020; 40: 2644-62.
 44. Tornusciolo DR, Schmidt RE, Roth KA. Simultaneous detection of TDT-mediated dUTP-biotin nick end-labeling (TUNEL)-positive cells and multiple immunohistochemical markers in single tissue sections. *Biotechniques.* 1995; 19: 800-5.
 45. Grinblat GA, Khan RS, Dine K, Wessel H, Brown L, Shindler KS. RGC Neuroprotection Following Optic Nerve Trauma Mediated By Intranasal Delivery of Amnion Cell Secretome. *Invest Ophthalmol Vis Sci.* 2018; 59: 2470-7.
 46. Liu H, Zhang J, Xu X, Lu S, Yang D, Xie C, et al. SARM1 promotes neuroinflammation and inhibits neural regeneration after spinal cord injury through NF- κ B signaling. *Theranostics.* 2021; 11: 4187-206.
 47. Compston A, Coles A. Multiple sclerosis. *Lancet.* 2008; 372: 1502-17.
 48. Zhang F, Zhang Y, Yang T, Ye ZQ, Tian J, Fang HR, et al. Scopolestin Suppresses Activation of Dendritic Cells and Pathogenesis of Experimental Autoimmune Encephalomyelitis by Inhibiting NF- κ B Signaling. *Front Pharmacol.* 2019; 10: 863.
 49. Coppolino GT, Marangon D, Negri C, Menichetti G, Fumagalli M, Gelosa P, et al. Differential local tissue permissiveness influences the final fate of GPR17-expressing oligodendrocyte precursors in two distinct models of demyelination. *Glia.* 2018; 66: 1118-30.
 50. Tassoni A, Farkhondeh V, Itoh Y, Itoh N, Sofroniew MV, Voskuhl RR. The astrocyte transcriptome in EAE optic neuritis shows complement activation and reveals a sex difference in astrocytic C3 expression. *Sci Rep.* 2019; 9: 10010.
 51. Manogaran P, Samardzija M, Schad AN, Wicki CA, Walker-Egger C, Rudin M, et al. Retinal pathology in experimental optic neuritis is characterized by retrograde degeneration and gliosis. *Acta Neuropathol Commun.* 2019; 7: 116.
 52. Shen X, Xu X, Xie C, Liu H, Yang D, Zhang J, et al. YAP promotes the proliferation of neuroblastoma cells through decreasing the nuclear location of p27(Kip1) mediated by Akt. *Cell Prolif.* 2020; 53: e12734.
 53. Shindler KS, Ventura E, Dutt M, Rostami A. Inflammatory demyelination induces axonal injury and retinal ganglion cell apoptosis in experimental optic neuritis. *Exp Eye Res.* 2008; 87: 208-13.
 54. Fan F, He Z, Kong LL, Chen Q, Yuan Q, Zhang S, et al. Pharmacological targeting of kinases MST1 and MST2 augments tissue repair and regeneration. *Sci Transl Med.* 2016; 8: 352ra108.
 55. Triastuti E, Nugroho AB, Zi M, Prehar S, Kohar YS, Bui TA, et al. Pharmacological inhibition of Hippo pathway, with the novel kinase inhibitor XMU-MP-1, protects the heart against adverse effects during pressure overload. *Br J Pharmacol.* 2019; 176: 3956-71.
 56. Huang L, Li S, Dai Q, Zhang A, Yu Q, Du W, et al. Astrocytic Yes-associated protein attenuates cerebral ischemia-induced brain injury by regulating signal transducer and activator of transcription 3 signaling. *Exp Neurol.* 2020; 333: 113431.
 57. Constantinescu CS, Farooqi N, O'Brien K, Gran B. Experimental autoimmune encephalomyelitis (EAE) as a model for multiple sclerosis (MS). *Br J Pharmacol.* 2011; 164: 1079-106.
 58. Uesugi N, Kimura Y, Yamashita T. Suppression of the p75 receptor signal attenuates the effect of ephrin-B3 and promotes axonal regeneration of the injured optic nerve. *Cell Death Dis.* 2013; 4: e557.
 59. Zhang CJ, Jiang M, Zhou H, Liu W, Wang C, Kang Z, et al. TLR-stimulated IRAK4 activates caspase-8 inflammasome in microglia and promotes neuroinflammation. *J Clin Invest.* 2018; 128: 5399-412.
 60. Tripathi RB, Rivers LE, Young KM, Jamen F, Richardson WD. NG2 glia generate new oligodendrocytes but few astrocytes in a murine experimental autoimmune encephalomyelitis model of demyelinating disease. *J Neurosci.* 2010; 30: 16383-90.
 61. Wheeler MA, Clark IC, Tjon EC, Li Z, Zandee SEJ, Couturier CP, et al. MAFG-driven astrocytes promote CNS inflammation. *Nature.* 2020; 578: 593-9.
 62. Lavrnja I, Savic D, Bjelobaba I, Dacic S, Bozic I, Parabucki A, et al. The effect of ribavirin on reactive astrogliosis in experimental autoimmune encephalomyelitis. *J Pharmacol Sci.* 2012; 119: 221-32.
 63. Krämer TJ, Hack N, Brühl TJ, Menzel L, Hummel R, Griemert EV, et al. Depletion of regulatory T cells increases T cell brain infiltration, reactive astrogliosis, and interferon- γ gene expression in acute experimental traumatic brain injury. *J Neuroinflammation.* 2019; 16: 163.
 64. Gasque P, Jones J, Singhrao SK, Morgan B. Identification of an astrocyte cell population from human brain that expresses perforin, a cytotoxic protein implicated in immune defense. *J Exp Med.* 1998; 187: 451-60.
 65. Lavado A, Park JY, Paré J, Finkelstein D, Pan H, Xu B, et al. The Hippo Pathway Prevents YAP/TAZ-Driven Hypertranscription and Controls Neural Progenitor Number. *Dev Cell.* 2018; 47: 576-91.e8.
 66. Kim JY, Park R, Lee JH, Shin J, Nickas J, Kim S, et al. Yap is essential for retinal progenitor cell cycle progression and RPE cell fate acquisition in the developing mouse eye. *Dev Biol.* 2016; 419: 336-47.
 67. Yasuda D, Kobayashi D, Akahoshi N, Ohto-Nakanishi T, Yoshioka K, Takuwa Y, et al. Lysophosphatidic acid-induced YAP/TAZ activation promotes developmental angiogenesis by repressing Notch ligand Dll4. *J Clin Invest.* 2019; 129: 4332-49.
 68. Mi H, Barres BA. Purification and characterization of astrocyte precursor cells in the developing rat optic nerve. *J Neurosci.* 1999; 19: 1049-61.
 69. Sun D. Visualizing Astrocytes of the Optic Nerve. *Methods Mol Biol.* 2018; 1695: 269-86.
 70. Abbott NJ. Inflammatory mediators and modulation of blood-brain barrier permeability. *Cell Mol Neurobiol.* 2000; 20: 131-47.
 71. da Cruz-Höfling MA, Raposo C, Verinaud L, Zago GM. Neuroinflammation and astrocytic reaction in the course of Phoneutria nigriventris (armed-spider) blood-brain barrier (BBB) opening. *Neurotoxicology.* 2009; 30: 636-46.
 72. Elahy M, Jackaman C, Mamo JC, Lam V, Dhaliwal SS, Giles C, et al. Blood-brain barrier dysfunction developed during normal aging is associated with inflammation and loss of tight junctions but not with leukocyte recruitment. *Immun Ageing.* 2015; 12: 2.
 73. Cekanaviciute E, Fathali N, Doyle KP, Williams AM, Han J, Buckwalter MS. Astrocytic transforming growth factor-beta signaling reduces subacute neuroinflammation after stroke in mice. *Glia.* 2014; 62: 1227-40.
 74. Cekanaviciute E, Dietrich HK, Axtell RC, Williams AM, Egusquiza R, Wai KM, et al. Astrocytic TGF- β signaling limits inflammation and reduces neuronal damage during central nervous system Toxoplasma infection. *J Immunol.* 2014; 193: 139-49.
 75. Diniz LP, Tortelli V, Matias I, Morgado J, Bergamo Araujo AP, Melo HM, et al. Astrocyte Transforming Growth Factor Beta 1 Protects Synapses against A β Oligomers in Alzheimer's Disease Model. *J Neurosci.* 2017; 37: 6797-809.

76. Shull MM, Ormsby I, Kier AB, Pawlowski S, Diebold RJ, Yin M, et al. Targeted disruption of the mouse transforming growth factor-beta 1 gene results in multifocal inflammatory disease. *Nature*. 1992; 359: 693-9.
77. Huh HD, Kim DH, Jeong HS, Park HW. Regulation of TEAD Transcription Factors in Cancer Biology. *Cells*. 2019; 8.
78. Hiemer SE, Szymaniak AD, Varelas X. The transcriptional regulators TAZ and YAP direct transforming growth factor β -induced tumorigenic phenotypes in breast cancer cells. *J Biol Chem*. 2014; 289: 13461-74.
79. Lee MJ, Byun MR, Furutani-Seiki M, Hong JH, Jung HS. YAP and TAZ regulate skin wound healing. *J Invest Dermatol*. 2014; 134: 518-25.